© 2017. Published by The Company of Biologists Ltd | Development (2017) 144, 2640-2651 doi:10.1242/dev.147231

RESEARCH ARTICLE

Antagonistic regulation of the second mitotic wave by Eyes absent-Sine oculis and Combgap coordinates proliferation and specification in the *Drosophila* retina

Trevor L. Davis[1] and Ilaria Rebay[1,2,*]

ABSTRACT

The transition from proliferation to specification is fundamental to the development of appropriately patterned tissues. In the developing *Drosophila* eye, Eyes absent (Eya) and Sine oculis (So) orchestrate the progression of progenitor cells from asynchronous cell division to G_1 arrest and neuronal specification at the morphogenetic furrow. Here, we uncover a novel role for Eya and So in promoting cell cycle exit in the second mitotic wave (SMW), a synchronized, terminal cell division that occurs several hours after passage of the furrow. We show that Combgap (Cg), a zinc-finger transcription factor, antagonizes Eya-So function in the SMW. Based on the ability of Cg to attenuate Eya-So transcriptional output *in vivo* and in cultured cells and on meta analysis of their chromatin occupancy profiles, we speculate that Cg limits Eya-So activation of select target genes posterior to the furrow to ensure properly timed mitotic exit. Our work supports a model in which context-specific modulation of transcriptional activity enables Eya and So to promote both entry into and exit from the cell cycle in a distinct spatiotemporal sequence.

KEY WORDS: Eye development, Cell cycle, Transcription factor, Retinal determination gene network, Mitotic exit

INTRODUCTION

Development of a functional organ requires coordination of proliferation with specification, differentiation, and morphogenesis. The capacity to divide typically inversely correlates with the progress of a cell toward terminal differentiation, such that mitotic cells are unspecified whereas differentiating cells have permanently exited the cell cycle (Buttitta and Edgar, 2007; Zhu and Skoultchi, 2001). Although many of the signaling pathways and transcription factors that direct these transitions have been identified, how inputs that promote and inhibit the cell cycle are balanced to schedule mitosis according to context is poorly understood (Brown et al., 2003; Buttitta and Edgar, 2007; Devès and Bourrat, 2012; Zhu and Skoultchi, 2001).

The unique spatiotemporal pattern of proliferation and differentiation in the *Drosophila* eye imaginal disc makes it an ideal model with which to study the underlying regulation. Prior to the third larval instar, asynchronous proliferation generates the pool of progenitor cells from which the different retinal cell types will be specified (Kumar, 2011). Differentiation begins when a burst of Decapentaplegic (Dpp) and Hedgehog (Hh) signaling at the posterior margin arrests cells in G_1 phase of the cell cycle and initiates the morphogenetic furrow (MF) (Chanut and Heberlein, 1997; Curtiss and Mlodzik, 2000; Dominguez and Hafen, 1997; Firth and Baker, 2005; Greenwood and Struhl, 1999; Horsfield et al., 1998; Ready et al., 1976; Vrailas and Moses, 2006; Wolff and Ready, 1991). As the MF propagates anteriorly across the eye field, arrested progenitor cells are either recruited into photoreceptor preclusters and specified as R8, R2, R5, R3 and R4 neurons or undergo one final synchronized round of mitosis known as the second mitotic wave (SMW) (Wolff and Ready, 1991). Progenitors that divide in the SMW adopt either an R1, R6 or R7 photoreceptor fate or the ommatidial accessory cone, pigment, and bristle fates (Wolff and Ready, 1991).

The retinal determination gene network (RDGN), which is composed of the transcription factors Eyeless (Ey), Eyes absent (Eya), Sine oculis (So) and Dachshund (Dac), governs the transition between proliferation and specification that occurs around the MF (Kumar, 2009). Anterior to the MF, coexpression of Ey with the transcription factors Homothorax (Hth), Yorkie and Teashirt promotes proliferation of the unspecified retinal precursors (Bessa et al., 2002; Lopes and Casares, 2010; Peng et al., 2009). Induction of Dpp and Hh signaling then represses Hth, enabling the onset of Dac, Eya and So expression (Bessa et al., 2002; Chen et al., 1999; Curtiss and Mlodzik, 2000; Halder et al., 1998; Lopes and Casares, 2010; Niimi et al., 1999; Pappu, 2003; Pappu et al., 2005; Salzer and Kumar, 2009). Dac interferes with the pro-proliferative transcriptional complexes to terminate mitogenic activity and permit differentiation, while Eya and So, operating as a bipartite transcription factor, take control of the cell cycle by activating a burst of *string* (*stg*) transcription that forces cells into M phase and prepares them for coordinated G_1 arrest (Brás-Pereira et al., 2015; Jemc and Rebay, 2007; Pignoni et al., 1997). Shortly thereafter, Eya-So first cooperates with Ey to activate *atonal* expression and initiate neuronal specification and then directly represses *ey* transcription to stabilize the suppression of the earlier proliferation program in the differentiating cells (Atkins et al., 2013; Zhang et al., 2006; Zhou et al., 2014).

After recruitment of the photoreceptor preclusters, a new combination of signaling and transcription factor inputs reinitiates the cell cycle, directing the remaining progenitors to undergo a single, synchronized and final division. Dpp, Hh, Notch and EGFR signaling all promote SMW proliferation, with antagonistic regulation of *stg* expression by the transcriptional activator and EGFR effector Pointed (Pnt) and the transcriptional repressor Tramtrack (Ttk) controlling the timing of M-phase entry (Baker and Yu, 2001; Baonza and Freeman, 2005; Baonza et al., 2002; Duman-Scheel et al., 2002; Firth and Baker, 2005, 2007; Sukhanova and

[1]Committee on Development, Regeneration, and Stem Cell Biology, University of Chicago, Chicago, IL 60637, USA. [2]Ben May Department for Cancer Research, University of Chicago, Chicago, IL 60637, USA.

*Author for correspondence (irebay@uchicago.edu)

I.R., 0000-0002-2444-3864

Received 23 November 2016; Accepted 8 June 2017

Development (2017) 144, 2640-2651 doi:10.1242/dev.147231

Du, 2008; Vrailas and Moses, 2006; Yang and Baker, 2003, 2006). Whether these are the only SMW regulators and how their activities are tuned to ensure that most unspecified precursors divide once with the correct timing is unknown and, in particular, the role of Eya-So has not yet been explored.

Here, we present evidence that antagonism between Eya-So and the transcription factor Combgap (Cg) helps to direct SMW proliferation in the *Drosophila* retina. Our data suggest that Eya-So stabilizes cell cycle exit to limit the number of mitoses undertaken by precursor cells in the SMW. By contrast, Cg promotes SMW proliferation such that its loss leads to a failure to generate sufficient precursors to assemble the complete eye. Mutual genetic antagonism between Eya-So and Cg suggests that their interaction contributes to the balance between positive and negative inputs that restricts precursor cells to a single mitosis after the MF passes. Mechanistically, we propose that Cg opposes Eya-So transcriptional activity, as Cg limits the ability of Eya-So to activate target genes both *in vivo* and in S2 cell-based transcription assays. Together, our results identify the first negative regulator of Eya-So transcriptional activity, uncover a novel context in which Eya-So controls the cell cycle, and bolster the model that balanced positive and negative transcriptional inputs calibrate the rate of SMW proliferation.

RESULTS

Eya-So limits SMW proliferation

Although Eya-So is known to contribute to the control of proliferation and cell cycle arrest at the onset of the MF (Jemc and Rebay, 2007; Karandikar et al., 2014; Lopes and Casares, 2015), its role in regulating the subsequent coordinated precursor cell mitosis known as the SMW has not been investigated. Because null clones of *eya* or *so* block MF progression (Pignoni et al., 1997), precluding analysis of the SMW, we instead used *GMR-GAL4* to express *UAS-RNAi* transgenes targeting their transcripts in all cells posterior to the MF. eya^{RNAi} strongly knocked down its target, as judged by a >85% reduction in Eya protein levels when driven with *GMR-GAL4* and a ∼65% penetrant 'eyeless' phenotype (with only small patches of retinal tissue in the remaining 35%) when driven with *ey-GAL4* (Fig. S1 and see Fig. 2G). Using anti-phosphorylated histone H3 (PH3) to mark mitotic cells, we found that knocking down *eya* or *so*, or both together, increased the rate of SMW mitosis by almost 50% (Fig. 1A-G). The lack of PH3 signal in ELAV-positive photoreceptors, together with the normal complement of ELAV-positive cells in the preclusters near the SMW, suggested that the extra PH3-positive nuclei resulted from progenitors undergoing extra mitoses, rather than from specified cells re-entering the cell cycle (Fig. 1H-K). The number of PH3-positive nuclei posterior to the SMW region did not increase (Fig. 1H-K). Consistent with *eya* operating as an SMW antagonist, reducing the dose of positive versus negative regulators of M phase suppressed and enhanced the $GMR{>}eya^{RNAi}$ phenotype, respectively (Fig. S2). We conclude that Eya-So participates in the transcriptional events that regulate mitosis at the SMW.

Next, we determined which phase of the cell cycle Eya-So regulates. Knocking down *eya* or *so* alone did not increase EdU incorporation at the SMW (Fig. 1L-N). However, depleting both expanded the domain of SMW cells in S phase (compare red brackets, Fig. 1L-O). Furthermore, knocking down *so* initiated ectopic S phases in cells posterior to the SMW, and expressing eya^{RNAi} exacerbated this phenotype (cyan brackets, Fig. 1N,O). The loss of ELAV-positive cells posterior to the SMW in eya^{RNAi}, so^{RNAi} discs (Fig. 1K), together with the increased EdU incorporation relative to that in the *so* knockdown alone (Fig. 1N,O), suggests that failure to stabilize the post-mitotic state of newly specified photoreceptors might contribute to the aberrant S-phase re-entry observed in double-knockdown retinas. Thus, Eya-So limits both S-phase and M-phase entry or progression and is required for cell cycle exit posterior to the MF.

Cg, a new *eya*-interacting transcription factor, limits Eya-So transcriptional output

That Eya is a transcriptional coactivator for So is well established (Ohto et al., 1999; Silver et al., 2003; Xu et al., 1997), and recent

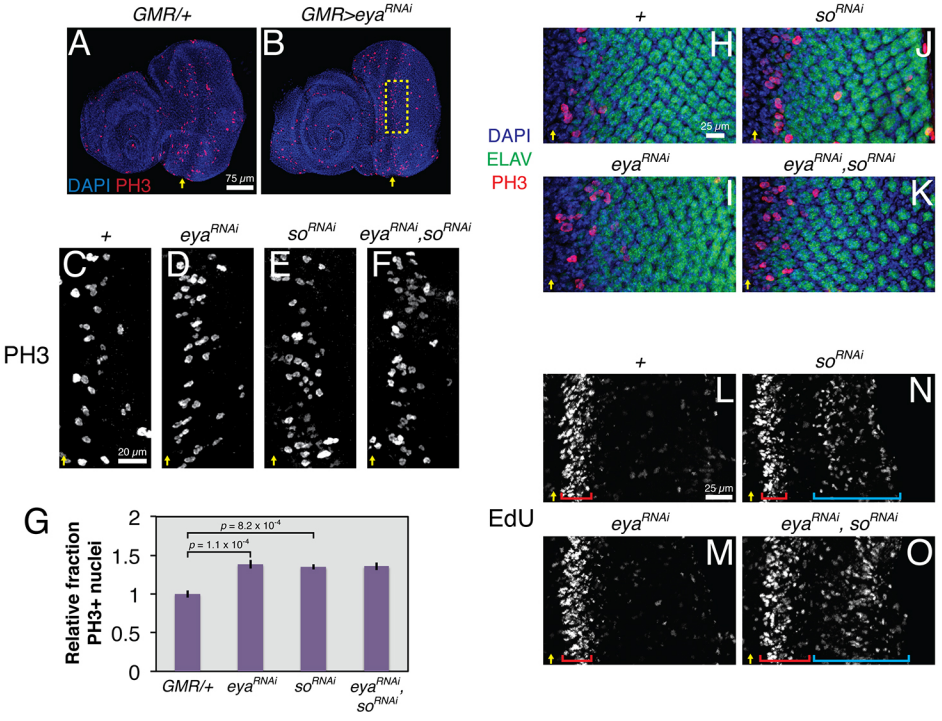

Fig. 1. Eya-So limits mitosis in the SMW. All images show representative late third instar eye-antennal imaginal discs. Yellow arrows mark the ventral edge of the MF. *UAS* transgenes were expressed with *GMR-GAL4*. (A,B) *eya* knockdown increases the number of $PH3^+$ nuclei in the SMW relative to the driver-alone control. (C-F) Magnified views of the SMW (boxed region in B) show increased numbers of $PH3^+$ nuclei in *eya* and *so* knockdown discs relative to driver-alone controls. Double knockdown does not further increase SMW mitoses. (G) Quantification of mitotic rates for genotypes in C-F ($n \geq 5$), calculated as the number of $PH3^+$ nuclei per μm of the MF and normalized to controls. (H-K) Inter-ommatidial spacing, marked by $ELAV^-$ DAPI-stained nuclei, is reduced and irregular in *eya* or *so* knockdown discs. In the double knockdown, a reduced number of $ELAV^+$ photoreceptors in the posterior produces the appearance of increased spacing. $PH3^+$ $ELAV^+$ nuclei were never detected. (L-O) EdU incorporation shows that *so* knockdown induces ectopic S phases (cyan brackets) posterior to the SMW (red brackets). *eya* knockdown enhances this phenotype.

Development (2017) 144, 2640-2651 doi:10.1242/dev.147231

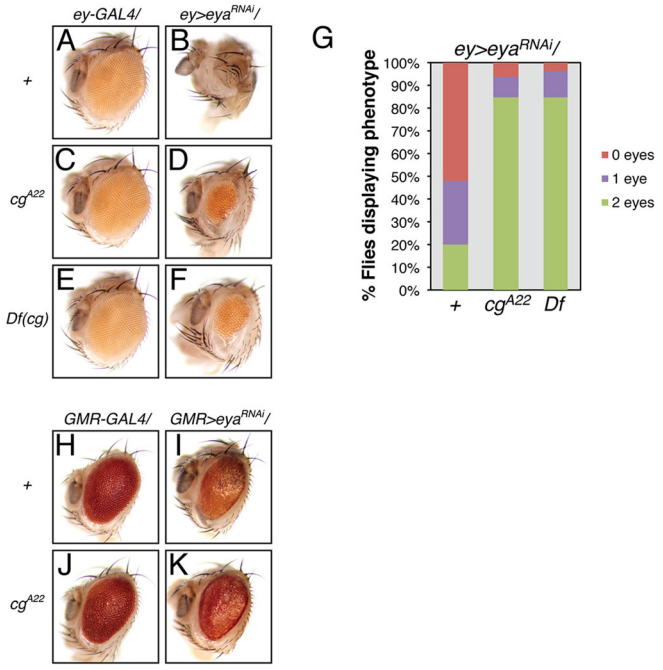

Fig. 2. *cg* antagonizes *eya* functions during retinal development. (A,B) Adult 'eyeless' phenotype associated with *ey-GAL4*-driven *eya* knockdown; eye loss is never observed in the driver-alone control. (C-F) *cg* heterozygosity, with either a null allele or a deficiency, suppresses the *ey>eya*^{RNAi} eyeless phenotype. (G) Quantification of penetrance of eye loss ($n \geq 91$ animals). Flies were scored for the presence of pigmented retinal tissue in both eye fields. (H,I) *GMR-GAL4*-driven *eya* knockdown reduces eye size and pigmentation; the driver alone produces a mild rough eye phenotype. (J,K) *cg* heterozygosity restores eye size and pigmentation in *eya* knockdown animals, but does not modify the driver-alone phenotype.

work has shown that Eya-So directly represses *ey* expression in differentiating cells posterior to the MF (Atkins et al., 2013). Extrapolating to the context of the SMW, Eya-So could limit proliferation by either activating the expression of negative regulators or repressing the expression of positive regulators, with different outputs presumably determined by its co-factors. However, of the few Eya-So binding partners studied to date, none is implicated in SMW regulation (Ahmed et al., 2012; Chen et al., 1997; Goldstein et al., 2005; Morillo et al., 2012; Pignoni et al., 1997). With the goals of expanding the repertoire of Eya-interacting factors and gaining additional insight into SMW regulation, we carried out a yeast two-hybrid screen using the conserved C-terminal Eya domain (ED) from *Drosophila* Eya as bait. Positive hits were tested for their ability to dominantly modify *eya* loss-of-function phenotypes anterior or posterior to the MF.

Among the most significant two-hybrid hits was a collection of clones whose overlap defined a span of eight zinc-fingers within the coding sequence of the transcription factor Cg. In follow-up genetic tests, heterozygosity for a *cg* null allele dominantly suppressed *eya* loss-of-function phenotypes. Specifically, in an *ey>eya*^{RNAi} hypomorphic background in which only 20% of adults developed bilateral eye tissue, reduction in *cg* dose increased that fraction to 80% (Fig. 2A-G), whereas in the *GMR>eya*^{RNAi} background it ameliorated the reduced pigmentation and increased adult eye size (Fig. 2H-K). These suppressive interactions classified *cg* as a genetic antagonist of *eya* both anterior and posterior to the MF.

cg was identified by Calvin Bridges and named to describe its roles in limiting the number of male sex combs and in patterning the wing veins (Lindsley and Zimm, 1992). Despite its ubiquitous expression in the eye-antennal imaginal disc (Fig. S3), its contributions to retinal development have not been described. Mechanistically, Cg works as a sequence-specific DNA-binding protein that contributes to recruitment of Polycomb repressive complexes (Ray et al., 2016), can organize the three-dimensional conformation of target loci (Hitrik et al., 2016), and is thought to activate and repress targets in the leg, wing and brain (Campbell and Tomlinson, 2000; Song et al., 2000; Svendsen et al., 2000). Based on this prior knowledge, Cg presented an intriguing candidate for a transcription factor that might influence the output of Eya-So.

To test this possibility, we asked whether Cg could alter Eya-So activity in an S2 cell-based transcription assay using an Eya-So-responsive transcriptional reporter carrying two copies of the *lozenge* minimal enhancer element (LMEE) (Yan et al., 2003) upstream of a minimal promoter and the coding sequence of firefly luciferase. Consistent with prior work (Mutsuddi et al., 2005; Silver et al., 2003), transient transfection of *eya* and *so* increased luciferase activity almost eightfold compared with the control (Fig. 3A). Co-transfection of *cg* with *eya* and *so* reduced reporter expression by half, a decrease made even more significant considering the slight activation observed when *cg* was transfected alone. Eya and So expression and subcellular localization were not affected by Cg overexpression, with all three proteins colocalizing in S2 cell nuclei (Fig. S4). The ability of Cg to reduce Eya-So activity was specific, as Cg did not reduce output from the transcriptional activator Pnt in similar assays (Fig. S5).

To examine whether Cg could antagonize Eya-So transcriptional output *in vivo*, we turned to a wing misexpression assay that has been used extensively to reveal regulatory relationships and to validate transcriptional targets of the RDGN (Chen et al., 1997; Halder et al., 1998; Jemc and Rebay, 2007; Morillo et al., 2012). In this experiment, *eya* misexpression along the anterior-posterior compartment boundary of the larval wing imaginal disc under the control of *dpp-GAL4* ectopically activates expression of the Eya-So target gene *dac* in a *so*-dependent manner. Cg is expressed uniformly throughout the wing disc (Campbell and Tomlinson, 2000; Svendsen et al., 2000), so we predicted that if Cg limits Eya-So transcriptional activity, then decreasing or increasing the *cg* dose should respectively enhance or reduce the ability of Eya to activate ectopic Dac expression. As previously reported (Morillo et al., 2012), *eya* misexpression under *dpp*^{40C6}*-GAL4* always induced a large dorsal patch of ectopic Dac (yellow arrow, Fig. 3B) and, at lower frequency, small clusters of Dac-positive cells in the wing pouch near the hinge (cyan arrows, compare Fig. 3B,C with E). Driving *eya* with a slightly stronger *GAL4* transgene (*dpp*^{57A1}*-GAL4*) also activated weak Dac expression throughout the *dpp* domain (orange arrow, Fig. 3F). *cg* heterozygosity in the *dpp*^{40C6}*>eya* background increased the number of clusters of wing pouch Dac-positive cells fourfold, suggesting that endogenous *cg* limits the ability of Eya-So to activate *dac* transcription (Fig. 3B-D). Consistent with this idea, co-overexpressing *cg* and *eya* eliminated induction of ectopic Dac in the dorsal wing or pouch, but did not alter the low-level Dac induced in the *dpp* domain (Fig. 3H). Eya protein levels and subcellular localization were unchanged by altering *cg* dose (Fig. S6), indicating that the antagonism of Eya-mediated Dac induction by Cg most likely reflects reduced Eya-So transcriptional activity.

In the course of the *cg* overexpression experiments, we noticed that *dpp>cg* alone disrupted wing disc morphology such that the discs were smaller, with aberrant folding patterns and partial loss of the physical asymmetry between anterior and posterior halves (Fig. 3G). Cg overexpression also reduced the ventral and medial

Development (2017) 144, 2640-2651 doi:10.1242/dev.147231

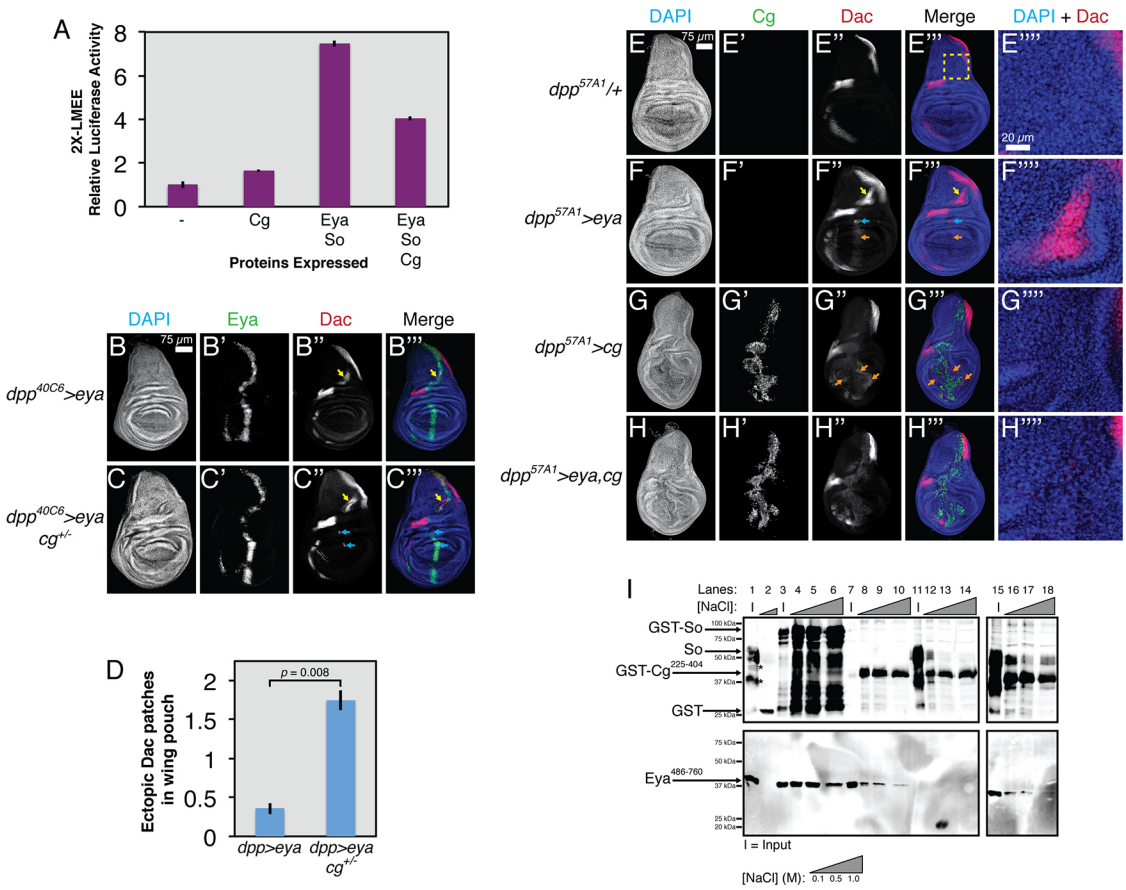

Fig. 3. Cg antagonizes transcriptional output from Eya-So. All stained tissues are late third instar wing imaginal discs (n>10 discs examined for all genotypes). (A) Cg limits the ability of Eya-So to activate LMEE-luciferase in S2 cell transcription assays (seven independent replicates). (B) *dpp-GAL4*-driven *eya* misexpression always induces ectopic Dac expression in the hinge (yellow arrows, compare with E″), but only occasionally in the pouch (not shown). (C) *cg* heterozygosity enhances the ability of *eya* to activate ectopic Dac in the pouch (cyan arrows). (D) Quantification of the number of ectopic Dac patches in the pouch for genotypes in B,C (n≥8). (E-H) A stronger *dpp-GAL4* driver. (E‴-H‴) Magnified views of the dorsal patch of ectopic Dac, as boxed in E‴. (E) Driver alone control showing the wild-type pattern of Dac expression. (F) *eya* misexpression induces ectopic Dac in the hinge (yellow arrow), pouch (blue arrow) and faintly throughout the *dpp* stripe in the pouch (orange arrow). (G) *cg* overexpression produces smaller wing discs with aberrant folds in the pouch and loss of the normal dorsal-ventral asymmetric shape and induces weak Dac expression in the pouch, both cell-autonomously and non-autonomously (orange arrows; note lack of overlap with Cg-expressing cells in the *dpp* stripe). (H) Wing discs co-overexpressing *cg* and *eya* no longer ectopically induce Dac in the hinge and pouch and display milder morphological disruptions than with *cg* overexpression alone. (I) *In vitro* GST pulldown assays show that Cg can directly bind Eya and can participate in a ternary complex with Eya-So (six independent replicates). Lanes 1-2, GST alone does not pull down So or FLAG-Eya$^{486\text{-}760}$. Full-length So runs as a triplet and the asterisk marks co-purifying degradation products. Lanes 3-6, GST-So pulls down FLAG-Eya$^{486\text{-}760}$. Lanes 7-10, GST-Cg$^{225\text{-}404}$ pulls down FLAG-Eya$^{486\text{-}760}$. Lanes 11-14, GST-Cg$^{225\text{-}404}$ does not effectively pull down So. Lanes 15-18, FLAG-Eya$^{486\text{-}760}$ increases the ability of GST-Cg$^{225\text{-}404}$ to pull down So.

patterns of endogenous Dac expression, presumably reflecting the altered morphology and fate of tissue in those regions. Weak, sometimes non-autonomous Dac misexpression was also observed in the anterior and posterior pouch compartments in these discs (orange arrows, Fig. 3G). Co-overexpression of *eya* with *cg* reduced the severity of *cg*-induced disruptions to overall disc morphology (Fig. 3H, Fig. S6), hinting that not only does Cg antagonize the transcriptional function of Eya, but also that Eya might reciprocally inhibit Cg.

Because we initially identified Cg as an Eya binding partner, we used *in vitro* pulldown assays with bacterially expressed proteins to test two different molecular models for how Cg might reduce Eya-So transcriptional activity. First, Eya bound to Cg might no longer interact with So. Alternatively, Cg might form a ternary complex with Eya-So that is less transcriptionally active than Eya-So alone. Because full-length Eya and Cg were poorly expressed and were largely insoluble and degraded (data not shown), we used smaller fragments that corresponded to the putative interaction domains identified by the two-hybrid screen. Confirming the two-hybrid result, GST-Cg$^{225\text{-}404}$ pulled down Eya$^{486\text{-}760}$, whereas GST alone did not (Fig. 3I, compare lanes 8-10 with lane 2). When GST-Cg$^{225\text{-}404}$ was mixed with full-length So, only an extremely weak interaction was detected (lanes 12-14). Addition of Eya$^{486\text{-}760}$ enabled GST-Cg$^{225\text{-}404}$ to pull down So, revealing formation of a ternary complex in which Eya bridges the interaction (lanes 16-18). We attempted to corroborate this result by co-immunoprecipitating the full-length proteins from transiently transfected S2 cells, but failed to detect the Eya-Cg interaction (data not shown), suggesting that Eya-Cg complexes might be more labile in cells than *in vitro*.

Cg promotes SMW proliferation and Eya-So opposes this activity

Returning to the developing retina, we examined whether *cg* genetically antagonizes *eya* function in the context of the SMW.

Development (2017) 144, 2640-2651 doi:10.1242/dev.147231

Indeed, *cg* heterozygosity dominantly suppressed the increased rate of SMW mitoses produced by *GMR>eya*^{RNAi} knockdown almost back to the wild-type level (Fig. 4A-C,G). Conversely, *cg* overexpression, which on its own produced a mild increase in PH3-positive SMW cells, enhanced the *eya* knockdown phenotype (Fig. 4D,E,H). Over the course of several experiments, only two animals in the latter experiment (Fig. 4D,H) and four overexpressing *cg* alone (Fig. 4E,H) survived to the late third instar, making statistical analyses difficult. However, the SMW proliferation rate of both *eya*^{RNAi}*,cg* larvae exceeded the expected result if *GMR>eya*^{RNAi} and *GMR>cg* additively interacted, supporting a model of genetic antagonism (2.16-fold and 2.61-fold increases; additive expectation 1.92-fold). These results both pinpoint the SMW as a developmental context in which *eya* and *cg* interact and suggest that *cg* positively regulates proliferation posterior to the MF.

To confirm the requirement of *cg* for the SMW, we examined the consequences of complete *cg* loss. As predicted, the SMW mitotic rate of *cg* null discs was half that of wild-type controls (Fig. 4I-K). Proliferation anterior to the MF (the first mitotic wave, or FMW) was unchanged, indicating that the requirement of *cg* for mitosis is specific to the SMW. Furthermore, *cg* mutants incorporated ~75% less EdU at the SMW than wild-type animals, suggesting that *cg* is required for efficient S-phase entry or progression (Fig. 4L,M,P). Heterozygosity for *eya* or *so* suppressed both the reduced EdU incorporation and lower proportion of PH3-positive nuclei in the SMW of *cg* null discs (Fig. 4L-U). These results suggest that the mutually antagonistic relationship between *cg* and *eya-so* helps set the correct SMW proliferation rate.

cg is required for normal eye-antennal disc morphology and cell survival

In addition to SMW phenotypes, we noted other defects in *cg* mutant eye-antennal discs. First, although neuronal specification appeared largely normal in *cg* null retinas as judged by the pattern of the marker ELAV (Fig. 5A,B), MF progression was delayed in the dorsal quarter such that the MF curved toward the posterior in this region (Fig. 5B,D,F, white arrows). This phenotype was variably penetrant in its severity, but the MF curvature consistently differed from that of the wild type (compare Fig. 5A,C,E with 5B,D,F). Second, an ectopic flap of tissue protruding from between the developing eye and antenna extended basally and posteriorly (Fig. 5B, D,F, red arrows). This flap was variable in size and sometimes reached underneath the MF, but we never observed defects in MF progression or differentiation that spatially correlated with apposition of the flap and retinal cells. The regional identity of the ectopic flap might be presumptive head cuticle based its location and expression of markers such as Cut (Fig. 5C-F) (Blochlinger et al., 1993; Weasner and Kumar, 2013). Third, *cg* mutant antennal discs frequently displayed a narrowed and misshapen antennal ring (Fig. 5C-F). Finally, *cg* loss induced abnormal apoptosis early in the third instar, with the greatest amount of cell death concentrated between the antenna and eye near the dorsal-ventral boundary, just anterior to the MF near the dorsal and ventral margins, and in the anterior of the antenna (Fig. 5G,H). This wave of apoptosis was largely complete by the late third instar. Thus, in addition to controlling SMW proliferation, *cg* appears to have roles in directing epithelial morphogenesis, stabilizing regional identities, and promoting cell survival.

Cell types generated by the SMW are progressively missing in *cg* mutants

The SMW generates a precursor pool sufficient for recruitment of photoreceptors 1, 6 and 7, cone cells, pigment cells and bristle cells.

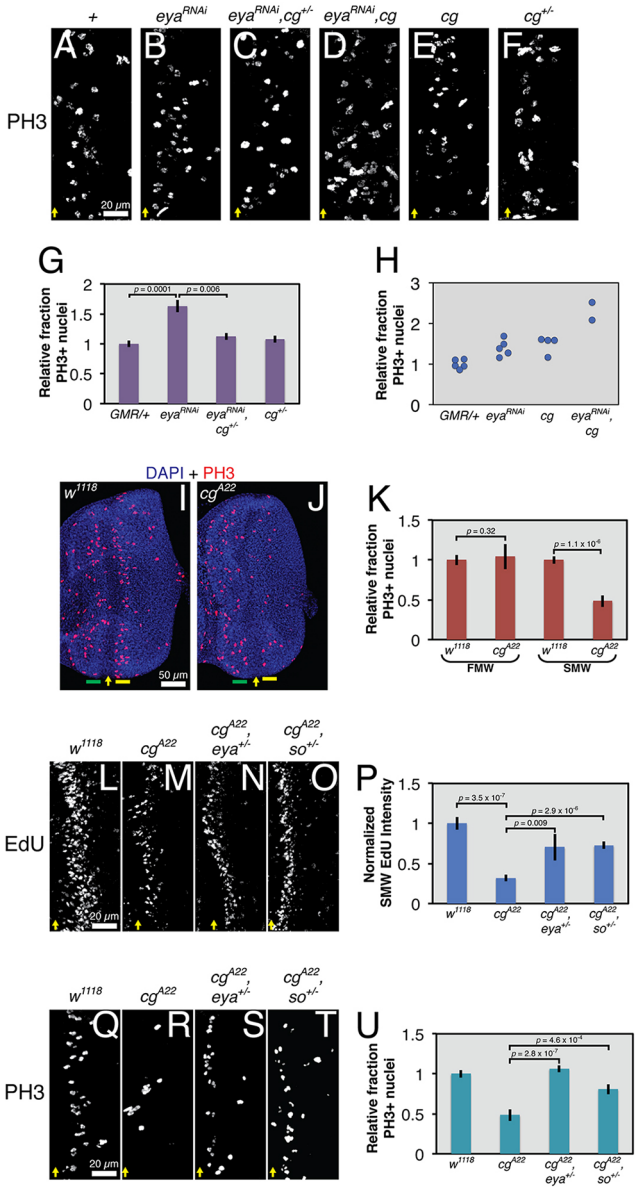

Fig. 4. Antagonistic inputs from *cg* and *eya* regulate SMW proliferation. All images show representative late third instar eye-antennal imaginal discs. Yellow arrows mark the ventral edge of the MF. *UAS* transgenes were expressed with *GMR-GAL4*. (A-D) *cg* heterozygosity suppresses and *cg* overexpression enhances the elevated SMW mitotic rate of *eya* knockdown animals. (E,F) *cg* overexpression modestly increases SMW proliferation, whereas heterozygosity has no effect. (G) Quantification of data in A,B,C,F ($n \geq 5$), calculated as the number of PH3$^+$ nuclei per μm of the MF and normalized to controls. (H) Quantification of data in A,B,D,E, calculated as in G. (I,J) Relative to control, *cg* loss reduces the number of PH3$^+$ nuclei in the SMW (yellow bar) but not in the first mitotic wave (FMW, green bar). (K) Quantification of data in I,J ($n \geq 9$), calculated as in G. (L-O) *cg* null discs incorporate less EdU at the SMW than wild-type controls, and *eya* or *so* heterozygosity dominantly suppresses this phenotype. (P) Quantification of background-subtracted fluorescent intensity of SMW EdU signal, normalized to the control intensity, for genotypes in L-O ($n \geq 5$). (Q-T) *eya* or *so* heterozygosity dominantly suppresses the reduction in PH3$^+$ nuclei in the SMW in *cg* mutants. (U) Quantification of data in Q-T ($n \geq 11$), calculated as in G. Actual PH3$^+$ counts for A-F and Q-T are provided in Table S1.

Thus, insufficient mitoses should cause loss of these retinal cell types, with the latest specified cells most significantly impacted as the precursors are depleted. To assess the complement of cell types

Development (2017) 144, 2640-2651 doi:10.1242/dev.147231

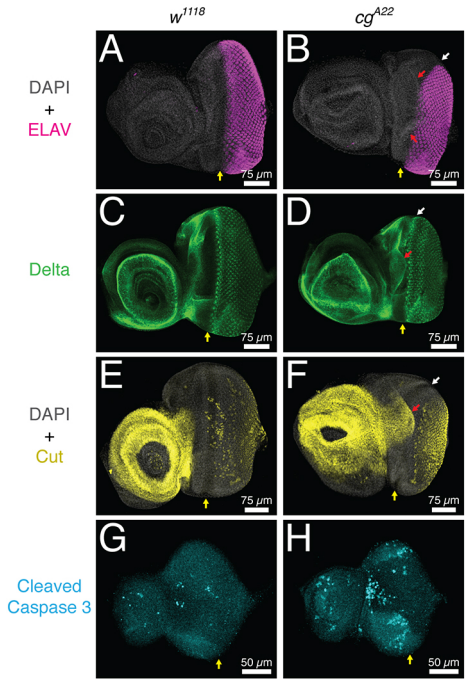

Fig. 5. *cg* is required for larval eye-antennal imaginal disc morphogenesis. All images show representative third instar eye-antennal imaginal discs. Yellow arrows mark the ventral edge of the MF. (A-F) Dorsal MF progression appears delayed (white arrows), presumptive head tissue is expanded (red arrows), and the overall morphology and folding of the antennal disc is irregular in late third instar *cg* mutants. (A,B) Photoreceptor specification, marked by ELAV expression, appears normal in *cg* mutants. (C,D) Delta is expressed in the expanded flap of tissue (red arrow) but otherwise appears normal in *cg* mutants. (E,F) Ectopic Cut expression is observed in the expanded flap of tissue (red arrow). Specification of Cut-positive cone cells appears normal in *cg* mutants. (G,H) Although overall *cg* disc morphology appears normal at the early third instar, increased apoptosis is detected in the antennal disc, at the antennal-eye boundary in the region where the extra flap of tissue will form, and in the lateral margins of the eye disc just anterior to the MF.

present in *cg* null retinal tissue, we stained with markers of various cell fates at several developmental time points. For analysis at pupal stages, we bypassed the larval lethality of cg^{A22} homozygotes with the cell lethal/*GMR-hid* system (Stowers and Schwarz, 1999) to generate retinas composed entirely of *cg* null tissue. First, recruitment of the ELAV-positive photoreceptors appeared nearly normal in *cg* mutants, with ommatidia only occasionally lacking a photoreceptor (Fig. 6A-D, yellow arrow). However, the ommatidia were packed more closely together and mildly disorganized in these third instar discs (Fig. 6A,B). Ommatidial organization appeared almost normal in the pupal *GMR-hid cg* clones, although occasionally the inter-ommatidial spacing was reduced, consistent with reduced SMW proliferation producing a smaller progenitor pool (Fig. 6A-D, white arrows). Second, and consistent with the ELAV results, Prospero (Pros)-positive R7 photoreceptors, which are recruited after the SMW, were rarely missing (Fig. 6E,F, yellow arrow), although their spacing and organization were abnormal. Third, ~20% of third instar *cg* mutant ommatidia had only three cone cells, as compared with the four present in wild type (Fig. 6G, H,J, yellow arrows), a frequency of loss consistent with the range reported for other mutants that reduce the SMW (Du et al., 1996). Focusing on the apical plane where the cone cell nuclei reside, ommatidial organization appeared essentially normal in the *cg* third instar disc (Fig. 6H). This observation suggests that irregular packing of the newly specified photoreceptor clusters (Fig. 6B′) might be a temporary aberration caused by proliferation defects and disorganization within the basal progenitor pool; restoration of a close to normal ommatidial lattice in the *cg* pupal disc (Fig. 6D′) is consistent with this idea. Fourth, *cg* mutant eyes contained fewer ELAV-positive bristle cells (Fig. 6M,N, yellow arrows) and Eya-positive pigment cells (Fig. 6O,P), supporting a progressive model of loss. Finally, *cg* whole-eye clones were smaller and rougher than their control counterparts (Fig. 6R,S), consistent with descriptions of mutants that ablate the SMW (de Nooij and Hariharan, 1995; Du et al., 1996; Xin et al., 2002).

Based on these analyses, we propose that *cg* mutant tissue, because of reduced SMW proliferation, might not generate adequate retinal precursors from which to assemble complete ommatidia. However, an alternate possibility is that the loss of cell fates is not connected to the reduced SMW proliferation, but rather reflects independent roles for *cg* in specifying or maintaining late-born cell fates. To distinguish these models, we focused on the cone cells. First, if *cg* were required to maintain cone cell fate, then we expected progressive loss of expression of cone cell markers. Although *cg* mutant ommatidia sometimes lacked a cone cell in the 48 h pupal disc (Fig. 6K,L, yellow arrows), the frequency of loss was not greater than in the third instar disc, arguing against a requirement for *cg* in cell fate maintenance. Second, we reasoned that because *eya* promotes cone cell specification (Karandikar et al., 2014), if the loss of cone cells in the *cg* mutant reflected an independent role in the signaling events that specify this fate, then heterozygosity for *eya* should enhance that phenotype. By contrast, if the reduced number of cone cells in the *cg* mutant stems from an insufficient progenitor pool, then because *eya* heterozygosity restored SMW proliferation in the *cg* mutant (Fig. 4L-U) it should also suppress the cone cell specification defect. Consistent with the latter prediction, *eya* heterozygosity suppressed cone cell loss in *cg* null discs (Fig. 6H-J). Reducing *eya* dosage also ameliorated pigment cell loss (Fig. 6P,Q) and adult eye roughness (Fig. 6S,T) in *cg* mutant tissue. Together, our results argue that insufficient SMW proliferation in the *cg* mutant compromises the ability to assemble complete ommatidia and confirm the requirement for *eya-cg* genetic antagonism in promoting normal retinal development.

Genes bound by both So and Cg are enriched for SMW regulators

Our finding that Cg can participate in the Eya-So complex *in vitro* and inhibit the ability of Eya-So to promote transcription motivated us to compare the published So and Cg genome-wide ChIP-seq profiles derived from third instar imaginal discs (Jusiak et al., 2014a, b; Ray et al., 2016). This analysis revealed that 61% of genes bound by Cg within 3 kb of their transcription start sites also contained a So peak in the same interval; conversely, Cg occupied 55% of genes bound by So (Fig. 7A). Co-occupied genes were enriched for gene ontology terms reflecting cell cycle regulation, as compared with loci bound by either protein alone (Fig. 7B). Of particular interest, a substantial population of genes experimentally shown to direct the SMW cell cycle were bound by both So and Cg (Fig. 7C). Consistent with a model in which Eya-So supports cell cycle exit by activating the transcription of cell cycle inhibitors, and Cg interferes with this regulation, we noted overlapping So and Cg occupancy at *dacapo* (*dap*), *roughex* (*rux*) and *Retinoblastoma-family protein* (*Rbf*) (Fig. 7D-F), although at subthreshold levels at the former two loci. *Rbf* is the most promising candidate, as *eya* overexpression has been reported to increase its transcription threefold (Jemc and Rebay, 2007) (Fig. S7). Collectively, these analyses are consistent

Development (2017) 144, 2640-2651 doi:10.1242/dev.147231

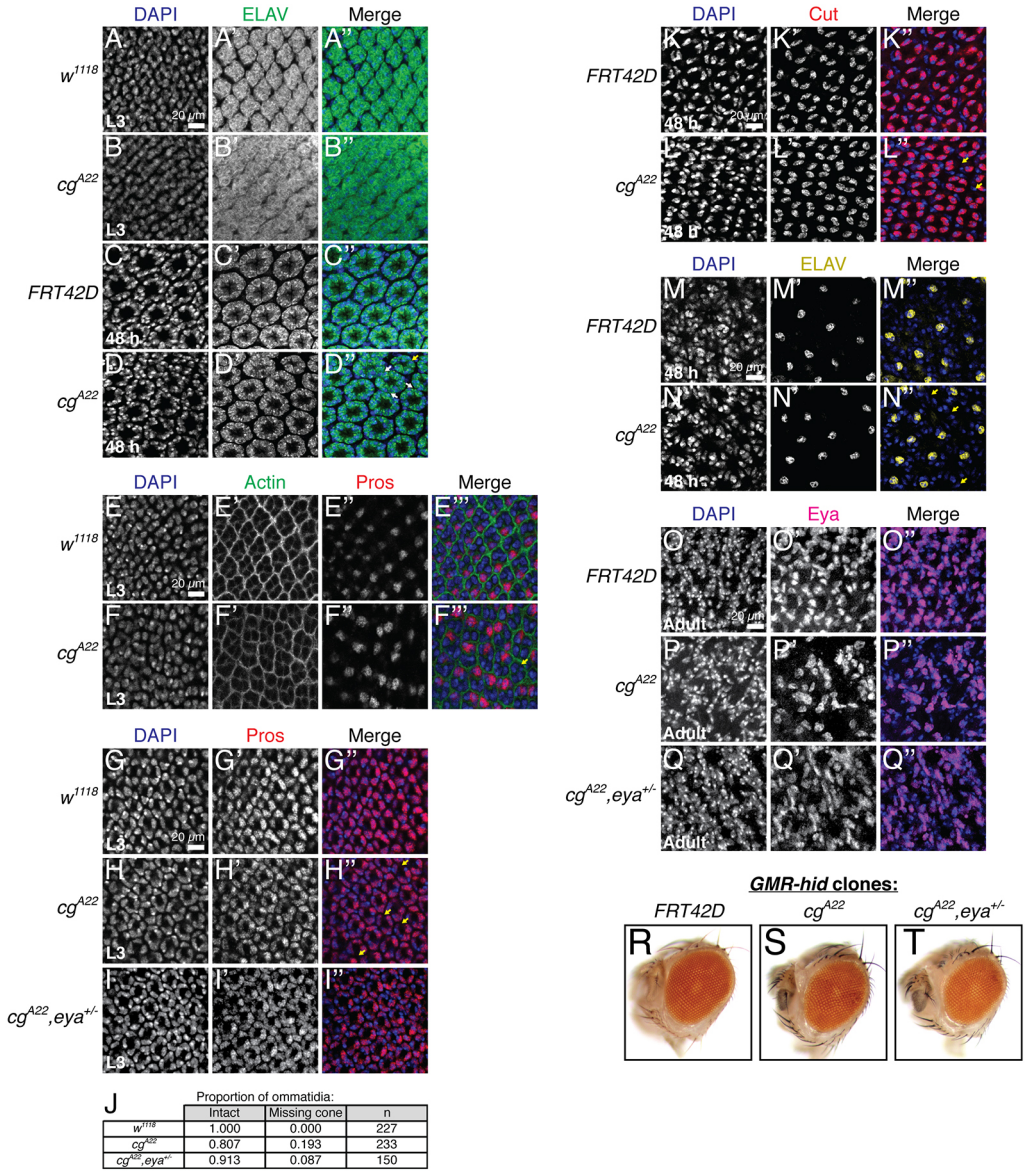

J

	Proportion of ommatidia:		
	Intact	Missing cone	n
w^{1118}	1.000	0.000	227
cg^{A22}	0.807	0.193	233
$cg^{A22},eya^{+/-}$	0.913	0.087	150

Fig. 6. Cell types specified after the SMW are progressively missing in *cg* null retinal tissue. All images show confocal projections of five or fewer slices at the apical-basal position of each cell type. When cell loss is claimed, complete confocal projections were examined to ensure that the cell in question was not mislocalized rather than absent. Third instar discs (L3) are from null *cg* mutants, while *cg* clones were used for pupal and adult time points. (A,B) Reduced inter-ommatidial space produces a disorganized ommatidial lattice in *cg* null third instar eye discs. (C,D) Patterning appears more regular in 48 h pupal whole-eye *cg* clones, although occasional reduction in inter-ommatidial distance (white arrows) and missing ELAV$^+$ photoreceptors (yellow arrow) are observed (D″). (E,F) Pros$^+$ R7 photoreceptors are irregularly spaced (F″) and occasionally missing (yellow arrow, F‴) in *cg* null L3 retinas. (G-I) Ommatidia with only three Pros$^+$ cone cells are frequently observed in *cg* null L3 eye discs (yellow arrows, H″) and *eya* heterozygosity suppresses this phenotype. (J) Quantification of the number of ommatidia containing the normal complement of cone cells (intact) or missing one cone cell for the genotypes in G-I. (K,L) Ommatidia with fewer Cut$^+$ cone cells are also observed in 48 h pupal *cg* null clones (yellow arrows, L″). (M,N) 48 h pupal *cg* null ommatidia sometimes lack ELAV$^+$ bristle cells (yellow arrows, N″). (O-Q) Significant loss and disorganization of the Eya$^+$ inter-ommatidial pigment cell lattice in adult *cg* clones as compared with control clones. Halving *eya* dosage suppresses pigment cell loss. (R-T) *eya* heterozygosity suppresses the mild rough eye phenotype of *cg* mutant retinal tissue.

with the hypothesis that Eya-So and Cg antagonistically control SMW proliferation by co-occupying and regulating the expression of genes that control this cell cycle.

DISCUSSION

Here we present evidence that Eya-So promotes exit of retinal precursors from the cell cycle after their final mitosis to permit their recruitment into ommatidia. Combined with published data, this finding suggests that the RDGN initiates both timely entry into and exit out of the cell cycle as retinal cells prepare to differentiate (Bessa et al., 2002; Brás-Pereira et al., 2015, 2016; Jemc and Rebay, 2007; Lopes and Casares, 2015). We also identify Cg as a novel positive regulator of the decision to re-enter S phase after G_1 arrest in the MF, and consequently expand the repertoire of transcription factors whose balanced positive and negative inputs link cell cycle progression with retinal specification. The ability of Cg to curb Eya-So transcriptional output, coupled with mutual genetic antagonism between these genes at the SMW, suggests that the dynamic assembly of uniquely composed Eya-So complexes with specific transcriptional activities coordinates proliferation with other cellular decisions in the developing eye.

Development (2017) 144, 2640-2651 doi:10.1242/dev.147231

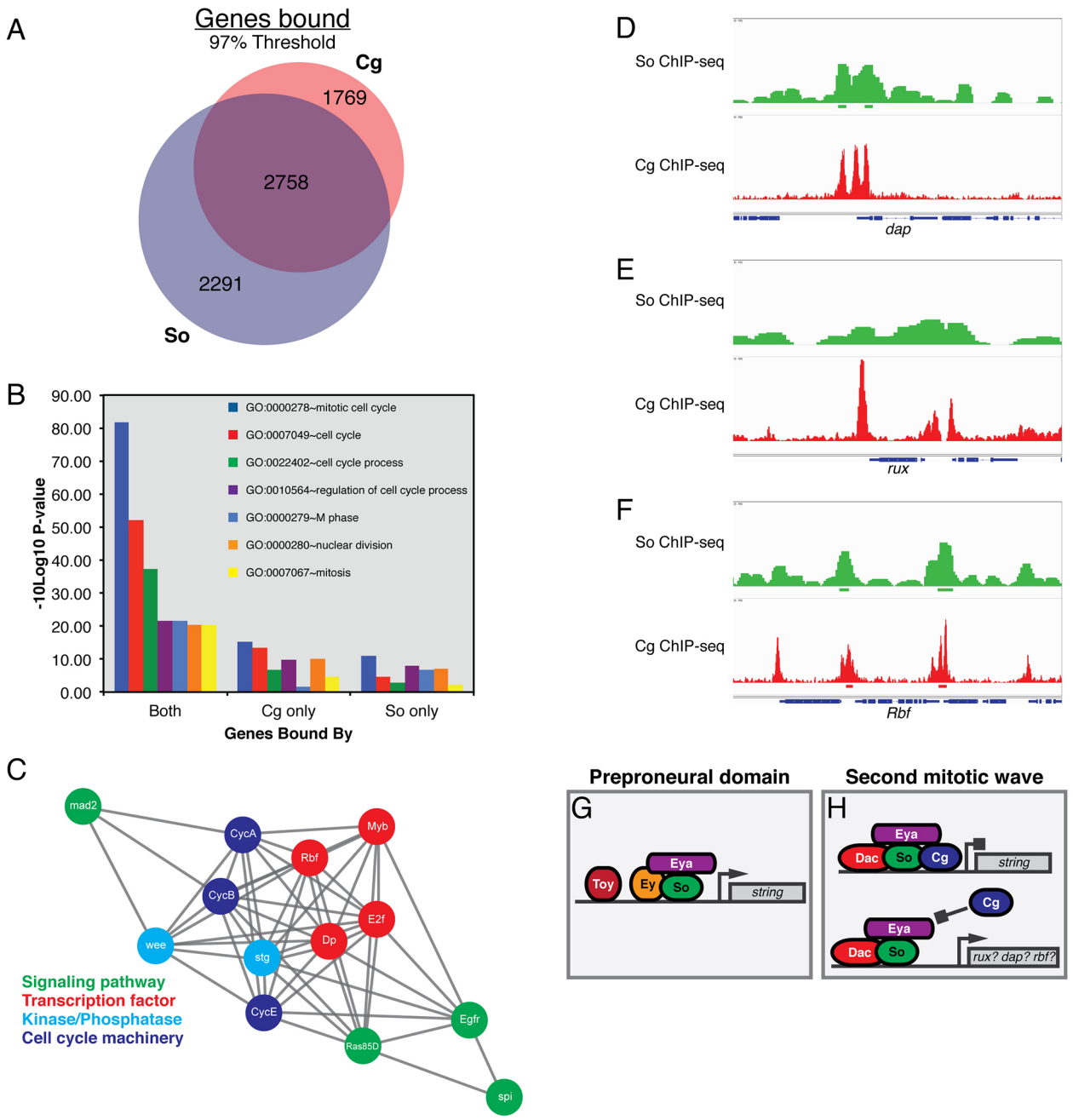

Fig. 7. Overlapping chromatin occupancy of So and Cg at genes that regulate the SMW. (A) The proportion of genes bound by So, Cg, or both at a 97% threshold. (B) Gene ontology (GO) terms associated with the cell cycle are enriched for the set of genes bound by both So and Cg. (C) Genes that control the SMW cell cycle are bound by So and Cg. Gray lines signify protein-protein, genetic, or computationally predicted interactions between genes as annotated by STRING. (D-F) So and Cg occupancy at *dap*, *rux* and *Rbf*. Peak calls are shown below the occupancy profiles. Peaks at *dap* and *rux* fell just under our stringent threshold. (G,H) RDGN transcription factors might assemble heterogeneous complexes at target loci to differentially regulate the cell cycle anterior and posterior to the morphogenetic furrow. 'Preproneural domain' refers to cells immediately anterior to the furrow, while 'second mitotic wave' denotes precursor cells undergoing their terminal division posterior to the furrow.

Our finding that Eya-So limits proliferation in the SMW suggests that regulation of the cell cycle by this transcriptional complex is more elaborate in two respects than is currently assumed. First, Eya-So does not promote proliferation in all contexts. Most prior studies conducted in flies and mammals have concluded that Eya and So family proteins stimulate proliferation during normal development and tumorigenesis. For example, Eya and Six proteins promote progression into S phase by activating transcription of the *Cyclin A1* or *Cyclin D1* genes (Coletta et al., 2004; Hua et al., 2014; Li et al., 2003, 2013), while *Drosophila* Eya-So stimulates M-phase entry by activating *stg* transcription (Jemc and Rebay, 2007). However, a recent study found that *eya* null cells in the MF inappropriately maintain *Cyclin B* expression, reflecting failure to arrest in G_1 (Karandikar et al., 2014), while we show that SMW cells with reduced Eya-So expression undergo extra mitoses, indicating that they cannot exit the cell cycle with the correct timing in preparation for terminal differentiation. Second, Eya-So does not control the cell cycle exclusively at the G_1-S and G_2-M transitions. Our experiments

Development (2017) 144, 2640-2651 doi:10.1242/dev.147231

reveal a novel third node of regulation by Eya-So: stabilization of cell cycle exit upon completion of M phase. Knocking down *eya* and *so* posterior to the MF induced ectopic DNA synthesis but not inappropriate M-phase entry, suggesting both that Eya-So prevents these precursors from proceeding into S phase and that the signaling and transcriptional environment once cells leave the SMW does not support progression further into the cell cycle. Many posterior cells lost ELAV expression in this experiment, consistent with either failed recruitment into ommatidia or an inability to stabilize neuronal fate upon re-entry into the cell cycle. We favor the latter interpretation, as neither *eya* nor *so* is required for larval photoreceptor differentiation (Jin et al., 2016).

These insights augment the model that the RDGN choreographs the sequence of cell cycle and developmental events that generates an eye. Early in retinal development, Ey cooperates with Hth and Teashirt to promote asynchronous proliferation (Bessa et al., 2002). Just before the MF initiates, another RDGN member, Dac, inhibits Hth-containing transcriptional complexes to terminate the early proliferation program, while Eya-So, Ey and Twin of Ey (Toy) activate *stg* transcription to push cells that have passed G_1 through M phase (Brás-Pereira et al., 2015; Jemc and Rebay, 2007; Lopes and Casares, 2015). A burst of Dpp and Hh signaling then synchronously arrests cells in the MF at G_1 (Escudero and Freeman, 2007; Firth and Baker, 2005; Horsfield et al., 1998; Vrailas and Moses, 2006). Dac collaborates with Dpp and Hh to initiate cell cycle exit at the MF (Brás-Pereira et al., 2015, 2016), and Eya also contributes (Karandikar et al., 2014), but it is unclear what molecular switch terminates Eya-So activation of *stg* transcription and balances the positive and negative inputs of retinal determination proteins to achieve this event. Transcriptional co-factors, such as Cg, are likely to tune Eya-So transcriptional activity, as we discuss below. Once the MF passes, Ey and Eya-So cooperate to promote *atonal* transcription and initiate neurogenesis (Zhang et al., 2006; Zhou et al., 2014). Our work attributes a final point of RDGN regulation of the cell cycle to Eya-So, which we show limits the remaining unspecified precursor cells in the SMW to a single division and maintains cell cycle arrest thereafter.

Illuminating the mechanisms that tailor the magnitude and direction of the effect of the RDGN on the cell cycle to specific developmental time points is an outstanding challenge. One emerging hypothesis is that Eya-So switches between activating and repressing its transcriptional targets, but the co-factors that drive these shifts and their relevance to proliferation are unknown. Specifically, So promotes *ey* transcription in retinal precursors, while Eya-So inhibits its expression in differentiating cells (Atkins et al., 2013). Similarly, Eya-So activates *stg* expression anterior to the MF, but not when cells arrest in G_1 (Jemc and Rebay, 2007). The inhibition by Cg of Eya-So transcriptional output *in vivo* and its participation in the complex *in vitro* make Cg a tantalizing candidate co-repressor that might terminate activation of transcription by Eya-So or initiate active repression to orchestrate the cell cycle. For example, Eya-So could contribute to cell cycle exit posterior to the MF by initiating transcription of genes that interfere with S-phase re-entry, such as *Rbf*, *rux* or *dap* (Buttitta et al., 2007; De Nooij et al., 1996; Lane et al., 1996; Ruggiero et al., 2012), but Cg might impede activation at these loci to permit cell cycle re-entry as cells enter the SMW. The enrichment of Cg and So co-occupancy at genes that govern proliferation (Fig. 7B-F), along with our finding that *cg* antagonizes the ability of *eya-so* to promote cell cycle exit, supports this hypothesis. The recent identification of Cg as a DNA-binding transcription factor that can recruit chromatin-remodeling Polycomb group (PcG) proteins (Ray et al., 2016) offers a potential repressive mechanism, and the specific links between epigenetic regulation and the RDGN are compelling subjects for future study.

While we favor a model in which Cg limits Eya-So function posterior to the MF and contributes to the transition from pro-mitotic activity to anti-proliferative function as the MF passes, all three proteins are broadly expressed in the larval retina (Fig. S3), indicating that some additional input must dictate this switch (Bonini et al., 1993; Campbell and Tomlinson, 2000; Cheyette et al., 1994; Svendsen et al., 2000). Intriguing candidates may be found among other retinal determination transcription factors. Ey and Toy coactivate *stg* transcription with Eya-So anterior to the MF (Jemc and Rebay, 2007; Lopes and Casares, 2015), but are not expressed at the SMW (Czerny et al., 1999; Halder et al., 1998). By contrast, Dac interferes with proliferation anterior to the MF (Brás-Pereira et al., 2015) and is required for cell cycle arrest after the SMW (Brás-Pereira et al., 2016). Therefore, perhaps Eya-So assembles activating transcriptional complexes with Ey and Toy at *stg* that override repressive Cg input in the preproneural domain, but interacts with Cg and Dac to inhibit *stg* transcription and maintain cell cycle exit posterior to the MF (Fig. 7G,H). Consistent with the hypothesis that Eya-So represses *stg* after the SMW, *so* knockdown ectopically activates a *stg* enhancer that is normally expressed only in the anterior (Lopes and Casares, 2015). Given the biochemical evidence for both Eya-So and Eya-Dac complexes (Chen et al., 1997; Jin and Mardon, 2016; Mutsuddi et al., 2005; Pignoni et al., 1997; Zhang et al., 2006), differential *stg* regulation anterior and posterior to the MF could reflect assembly of heterogeneous RDGN transcriptional complexes. However, posterior *ey* misexpression did not alter the rate of mitosis in the SMW (data not shown), indicating that Ey alone is not sufficient to reverse the direction of the effect of Eya-So on proliferation. Moreover, *ey* was not derepressed in *cg* clones posterior to the MF, and *cg* overexpression anterior to the MF did not repress *ey* (Fig. S8), arguing that Cg does not control proliferation by influencing Eya-So regulation at *ey*. Elucidating how the combinatorial action of unique RDGN protein complexes dictates enhancer specificity at *stg* and other loci to schedule cell cycle events is a rich topic for future study.

MATERIALS AND METHODS

Drosophila strains

UAS-eya^{RNAi} and *UAS-so*^{RNAi} were obtained from the Vienna *Drosophila* Resource Center. The following were from the Bloomington *Drosophila* Stock Center: *GMR-GAL4*^{Zipursky}, *pnt*$^{\Delta 88}$, *ttk*^{1e11}, *ey-GAL4*, *Df(2R)BSC401/CyO*, *dpp*^{40C6}*-GAL4*, *eya*^{Clift}, *so*^{3}, *ey-FLP;FRT42D,ubi-GFP/CyO*, *y*^{1}*,w*; FRT42D,y*$^{+}$*,GMR-hid,l(2)CL-R*^{1}*/Cyo;ey-GAL4,UAS-FLP* and *FRT42D*. Additional strains: *cg*^{422} (a gift of Gerard Campbell, University of Pittsburgh, PA, USA), *UAS-stg*^{RNAi} (Kyoto Stock Center), *dpp*^{57A1}*-GAL4* (Staehling-Hampton et al., 1994), *UAS-eya*^{I} (Hsiao et al., 2001), *UAS-eya*^{IIIa} (Hsiao et al., 2001) and *UAS-cg* (this work). For further details of *Drosophila* strains and genetics, see the supplementary Materials and Methods.

Immunohistochemistry and microscopy

Imaging was performed with a Zeiss LSM 510 or Zeiss LSM 880 confocal microscope, using 0.5 to 1.0 µm steps and projecting maximally through the desired tissue unless otherwise noted. See supplementary Materials and Methods for the antibodies used. *P*-values were calculated using two-tailed Student's *t*-tests of two-sample equal variance between the indicated genotypes, and data are plotted as mean±s.e.m. To image adult eyes, 3- to 5-day-old adult flies were decapitated and photographed with a Canon EOS Rebel camera fitted to a Leica dissecting microscope. Individual slices were merged using iSolution-Lite software (IMT-Digital).

Development (2017) 144, 2640-2651 doi:10.1242/dev.147231

In vitro pulldown assays

The $Cg^{225\text{-}404}$ fragment was PCR amplified from *cg* with 5′-ATAGGATCCCTGCTGCTTCACTCCACGGAGAGACC-3′ and 5′-AAACTCGAGGTTGGGATTGACGCCATTGTGCG-3′ and ligated into pGEX-4T-1. GST, So and Eya recombinant proteins were prepared and the pulldown assays performed as previously described (Morillo et al., 2012). See the supplementary Materials and Methods for details.

Transcription assays

2.25×10^6 *Drosophila* S2 cells plated in 12-well plates were transfected with 750 ng total plasmid DNA as described in the supplementary Materials and Methods. *cg* and *eya* were expressed constitutively under the *Actin5C* promoter, while *so* expression was controlled with the $CuSO_4$-inducible *Metallothionein* promoter (plasmid pRmHA-3; Silver et al., 2003).

Bioinformatic analysis of So and Cg ChIP-seq datasets

We obtained the genomic coordinates of the top 3% of peaks by height using the Integrated Genome Browser (Freese et al., 2016); this threshold is more stringent than either published set of peak calls (Jusiak et al., 2014a,b; Ray et al., 2016). A list of genomic coordinates ±3 kb from every transcription start site in the genome (assembly dm3) was generated using bedtools slop and merged with peak lists using bedtools intersect to produce lists of transcription start sites associated with peaks of So only, Cg only, or both So and Cg. Fig. 7A was generated using BioVenn (Hulsen et al., 2008), gene ontology terms were analyzed with the DAVID Functional Annotation tool (Huang et al., 2008, 2009), the protein-protein interaction network of genes co-bound by So and Cg was generated using STRING (Szklarczyk et al., 2015), and peaks were visualized with the Integrative Genomics Viewer (Thorvaldsdóttir et al., 2013).

Acknowledgements

We thank Gerard Campbell for *FRT42D,cg*^{A22} flies; Judith Kassis for sharing her lab's called Cg peaks; Jemma Webber, Nicelio Sanchez-Luege and Matt Hope for help with bioinformatics; Aaron Mitchell-Dick for initial exploration of yeast two-hybrid hits; members of the Justin Kumar, Wei Du and David Kovar labs for advice on the EdU protocol and pulldown experiments; Rick Fehon for the Delta and cleaved caspase 3 antibodies and the equipment to photograph adult eyes; current and former members of the I.R. and Fehon labs, Chip Ferguson, David Kovar, Doug Bishop and Jim Holaska for helpful discussions; and Matt Hope and Nicelio Sanchez-Luege for critiquing this manuscript.

Competing interests

The authors declare no competing or financial interests.

Author contributions

Conceptualization: I.R., T.L.D.; Methodology: I.R., T.L.D.; Validation: I.R., T.L.D.; Formal analysis: T.L.D.; Investigation: T.L.D.; Writing - original draft: I.R., T.L.D.; Writing - review & editing: I.R., T.L.D.; Visualization: I.R., T.L.D.; Supervision: I.R.; Project administration: I.R., T.L.D.; Funding acquisition: I.R.

Funding

This work was supported by National Institutes of Health (NIH) grant R01 EY12549 to I.R. and by the Genomics Core Facility through a University of Chicago Cancer Center Support Grant P30 CA014599. T.L.D. was supported by NIH T32 HD055164. Deposited in PMC for release after 12 months.

Supplementary information

Supplementary information available online at
http://dev.biologists.org/lookup/doi/10.1242/dev.147231.supplemental

References

Ahmed, M., Wong, E. Y. M., Sun, J., Xu, J., Wang, F. and Xu, P.-X. (2012). Eya1-Six1 interaction is sufficient to induce hair cell fate in the cochlea by activating Atoh1 expression in cooperation with Sox2. *Dev. Cell* **22**, 377-390.

Atkins, M., Jiang, Y., Sansores-Garcia, L., Jusiak, B., Halder, G. and Mardon, G. (2013). Dynamic rewiring of the Drosophila retinal determination network switches its function from selector to differentiation. *PLoS Genet.* **9**, e1003731.

Baker, N. E. and Yu, S.-Y. (2001). The EGF receptor defines domains of cell cycle progression and survival to regulate cell number in the developing Drosophila eye. *Cell* **104**, 699-708.

Baonza, A. and Freeman, M. (2005). Control of cell proliferation in the Drosophila eye by notch signaling. *Dev. Cell* **8**, 529-539.

Baonza, A., Murawsky, C. M., Travers, A. A. and Freeman, M. (2002). Pointed and Tramtrack69 establish an EGFR-dependent transcriptional switch to regulate mitosis. *Nat. Cell Biol.* **4**, 976-980.

Bessa, J., Gebelein, B., Pichaud, F., Casares, F. and Mann, R. S. (2002). Combinatorial control of Drosophila eye development by eyeless, homothorax, and teashirt. *Genes Dev.* **16**, 2415-2427.

Bischof, J., Maeda, R. K., Hediger, M., Karch, F. and Basler, K. (2007). An optimized transgenesis system for Drosophila using germ-line-specific phiC31 integrases. *Proc. Natl. Acad. Sci. USA* **104**, 3312-3317.

Blochlinger, K., Bodmer, R., Jan, L. Y. and Jan, Y. N. (1990). Patterns of expression of cut, a protein required for external sensory organ development in wild-type and cut mutant Drosophila embryos. *Genes Dev.* **4**, 1322-1331.

Blochlinger, K., Jan, L. Y. and Jan, Y. N. (1993). Postembryonic patterns of expression of cut, a locus regulating sensory organ identity in Drosophila. *Development* **450**, 441-450.

Bonini, N. M., Leiserson, W. M. and Benzer, S. (1993). The eyes absent gene: genetic control of cell survival and differentiation in the developing Drosophila eye. *Cell* **72**, 379-395.

Brás-Pereira, C., Casares, F. and Janody, F. (2015). The retinal determination gene dachshund restricts cell proliferation by limiting the activity of the Homothorax-Yorkie complex. *Development* **142**, 1470-1479.

Brás-Pereira, C., Potier, D., Jacobs, J., Aerts, S., Casares, F. and Janody, F. (2016). dachshund potentiates hedgehog signaling during Drosophila retinogenesis. *PLoS Genet.* **12**, e1006204.

Brown, G., Hughes, P. J. and Michell, R. H. (2003). Cell differentiation and proliferation–simultaneous but independent? *Exp. Cell Res.* **291**, 282-288.

Buttitta, L. A. and Edgar, B. A. (2007). Mechanisms controlling cell cycle exit upon terminal differentiation. *Curr. Opin. Cell Biol.* **19**, 697-704.

Buttitta, L. A., Katzaroff, A. J., Perez, C. L., de la Cruz, A. and Edgar, B. A. (2007). A double-assurance mechanism controls cell cycle exit upon terminal differentiation in Drosophila. *Dev. Cell* **12**, 631-643.

Campbell, G. L. and Tomlinson, A. (2000). Transcriptional regulation of the Hedgehog effector CI by the zinc-finger gene combgap. *Development* **127**, 4095-4103.

Campbell, G., Göring, H., Lin, T., Spana, E., Andersson, S. and Doe, C. Q. (1994). RK2, a glial-specific homeodomain protein required for embryonic nerve cord condensation and viability in Drosophila. *Development* **120**, 2957-2966.

Chanut, F. and Heberlein, U. (1997). Role of decapentaplegic in initiation and progression of the morphogenetic furrow in the developing Drosophila retina. *Development* **124**, 559-567.

Chen, R., Amoui, M., Zhang, Z. and Mardon, G. (1997). Dachshund and eyes absent proteins form a complex and function synergistically to induce ectopic eye development in Drosophila. *Cell* **91**, 893-903.

Chen, R., Halder, G., Zhang, Z. and Mardon, G. (1999). Signaling by the TGF-beta homolog decapentaplegic functions reiteratively within the network of genes controlling retinal cell fate determination in Drosophila. *Development* **126**, 935-943.

Cheyette, B. N. R., Green, P. J., Martin, K., Garren, H., Hartenstein, V. and Zipursky, S. L. (1994). The Drosophila sine oculis locus encodes a homeodomain-containing protein required for the development of the entire visual system. *Neuron* **12**, 977-996.

Coletta, R. D., Christensen, K., Reichenberger, K. J., Lamb, J., Micomonaco, D., Huang, L., Wolf, D. M., Müller-Tidow, C., Golub, T. R., Kawakami, K. et al. (2004). The Six1 homeoprotein stimulates tumorigenesis by reactivation of cyclin A1. *Proc. Natl. Acad. Sci. USA* **101**, 6478-6483.

Curtiss, J. and Mlodzik, M. (2000). Morphogenetic furrow initiation and progression during eye development in Drosophila: the roles of decapentaplegic, hedgehog and eyes absent. *Development* **1336**, 1325-1336.

Czerny, T., Halder, G., Kloter, U., Souabni, A., Gehring, W. J. and Busslinger, M. (1999). Twin of eyeless, a second Pax-6 gene of Drosophila, acts upstream of eyeless in the control of eye development. *Mol. Cell* **3**, 297-307.

de Nooij, J. C. and Hariharan, I. K. (1995). Uncoupling cell fate determination from patterned cell division in the Drosophila eye. *Science* **270**, 983-985.

de Nooij, J. C., Letendre, M. A. and Hariharan, I. K. (1996). A cyclin-dependent kinase inhibitor, dacapo, is necessary for timely exit from the cell cycle during Drosophila embryogenesis. *Cell* **87**, 1237-1247.

Devès, M. and Bourrat, F. (2012). Transcriptional mechanisms of developmental cell cycle arrest: problems and models. *Semin. Cell Dev. Biol.* **23**, 290-297.

Dominguez, M. and Hafen, E. (1997). Hedgehog directly controls initiation and propagation of retinal differentiation in the Drosophila eye. *Genes Dev.* **11**, 3254-3264.

Du, W. E. I., Vidal, M., Xie, J.-E. and Dyson, N. (1996). RBF, a novel RB-related gene that regulates E2F activity and interacts with cyclin E in Drosophila. *Genes Dev.* **10**, 1206-1218.

Duman-Scheel, M., Weng, L., Xin, S. and Du, W. (2002). Hedgehog regulates cell growth and proliferation by inducing Cyclin D and Cyclin E. *Nature* **417**, 299-304.

Escudero, L. M. and Freeman, M. (2007). Mechanism of G1 arrest in the Drosophila eye imaginal disc. *BMC Dev. Biol.* **13**, 1-13.

Fehon, R. G., Kooh, P. J., Rebay I., Regan, C. L., Xu T., Muskavitch M. A. T. and Artavanis-Tsakonas S. (1990). Molecular interactions between the protein

Development (2017) 144, 2640-2651 doi:10.1242/dev.147231

products of the neurogenic loci notch and Delta, two EGF-homologous genes in Drosophila. *Cell* **61**, 523-534.

Firth, L. C. and Baker, N. E. (2005). Extracellular signals responsible for spatially regulated proliferation in the differentiating Drosophila eye. *Dev. Cell* **8**, 541-551.

Firth, L. C. and Baker, N. E. (2007). Spitz from the retina regulates genes transcribed in the second mitotic wave, peripodial epithelium, glia and plasmatocytes of the Drosophila eye imaginal disc. *Dev. Biol.* **307**, 521-538.

Freese, N. H., Norris, D. C. and Loraine, A. E. (2016). Integrated genome browser: visual analytics platform for genomics. *Bioinformatics* **32**, 2089-2095.

Goldstein, R. E., Cook, O., Dinur, T., Pisanté, A., Karandikar, U. C., Bidwai, A. and Pisante, A. (2005). An eh1-like motif in odd-skipped mediates recruitment of groucho and repression in vivo. *Mol. Cell. Biol.* **25**, 10711-10720.

Greenwood, S. and Struhl, G. (1999). Progression of the morphogenetic furrow in the Drosophila eye: the roles of Hedgehog, Decapentaplegic and the Raf pathway. *Development* **126**, 5795-5808.

Halder, G., Callaerts, P., Flister, S., Walldorf, U., Kloter, U. and Gehring, W. J. (1998). Eyeless initiates the expression of both sine oculis and eyes absent during Drosophila compound eye development. *Development* **125**, 2181-2191.

Hitrik, A., Popliker, M., Gancz, D., Mukamel, Z., Lifshitz, A., Schwartzman, O., Tanay, A. and Gilboa, L. (2016). Combgap promotes ovarian niche development and chromatin association of EcR-binding regions in BR-C. *PLoS Genet.* **12**, e1006330.

Horsfield, J., Penton, A., Secombe, J., Hoffman, F. M. and Richardson, H. (1998). decapentaplegic is required for arrest in G1 phase during Drosophila eye development. *Development* **125**, 5069-5078.

Hsiao, F. C., Williams, A., Davies, E. L. and Rebay, I. (2001). Eyes absent mediates cross-talk between retinal determination genes and the receptor tyrosine kinase signaling pathway. *Dev. Cell* **1**, 51-61.

Hua, L., Fan, L., Aichun, W., Yongjin, Z., Qingqing, C. and Xiaojian, W. (2014). Inhibition of Six1 promotes apoptosis, suppresses proliferation, and migration of osteosarcoma cells. *Tumor Biol.* **35**, 1925-1931.

Huang, D. W., Sherman, B. T. and Lempicki, R. A. (2008). Systematic and integrative analysis of large gene lists using DAVID bioinformatics resources. *Nat. Protoc.* **4**, 44-57.

Huang, D. W., Sherman, B. T. and Lempicki, R. A. (2009). Bioinformatics enrichment tools: paths toward the comprehensive functional analysis of large gene lists. *Nucleic Acids Res.* **37**, 1-13.

Hulsen, T., de Vlieg, J. and Alkema, W. (2008). BioVenn – a web application for the comparison and visualization of biological lists using area-proportional Venn diagrams. *BMC Genomics* **9**, 488.

Jemc, J. and Rebay, I. (2007). Identification of transcriptional targets of the dual-function transcription factor/phosphatase eyes absent. *Dev. Biol.* **310**, 416-429.

Jin, M. and Mardon, G. (2016). Distinct biochemical activities of eyes absent during drosophila eye development. *Sci. Rep.* **6**, 23228.

Jin, M., Eblimit, A., Pulikkathara, M., Corr, S., Chen, R. and Mardon, G. (2016). Conditional knockout of retinal determination genes in differentiating cells in Drosophila. *FEBS J.* **283**, 2754-2766.

Jusiak, B., Karandikar, U. C., Kwak, S.-J., Wang, F., Wang, H., Chen, R. and Mardon, G. (2014a). Regulation of Drosophila eye development by the transcription factor Sine oculis. *PLoS ONE* **9**, e89695.

Jusiak, B., Wang, F., Karandikar, U. C., Kwak, S.-J., Wang, H., Chen, R. and Mardon, G. (2014b). Genome-wide DNA binding pattern of the homeodomain transcription factor Sine oculis (So) in the developing eye of Drosophila melanogaster. *Genomics Data* **2**, 153-155.

Karandikar, U. C., Jin, M., Jusiak, B., Kwak, S. J., Chen, R. and Mardon, G. (2014). Drosophila eyes absent is required for normal cone and pigment cell development. *PLoS ONE* **9**, e102143.

Kumar, J. P. (2009). The molecular circuitry governing retinal determination. *Biochim. Biophys. Acta* **1789**, 306-314.

Kumar, J. P. (2011). My what big eyes you have: how the drosophila retina grows. *Dev. Neurobiol.* **71**, 1133-1152.

Lane, M. E., Sauer, K., Wallace, K., Jan, Y. N., Lehner, C. F. and Vaessin, H. (1996). Dacapo, a cyclin-dependent kinase inhibitor, stops cell proliferation during Drosophila development. *Cell* **87**, 1225-1235.

Li, X., Oghi, K. A., Zhang, J., Krones, A., Bush, K. T., Glass, C. K., Nigam, S. K., Aggarwal, A. K., Maas R., Rose D. W. et al. (2003). Eya protein phosphatase activity regulates Six1 – Dach – Eya transcriptional effects in mammalian organogenesis. *Nature* **426**, 247-254.

Li, Z., Tian, T., Lv, F., Chang, Y., Wang, X., Zhang, L., Li, X., Li, L., Ma, W., Wu, J. et al. (2013). Six1 promotes proliferation of pancreatic cancer cells via upregulation of cyclin D1 expression. *PLoS ONE* **8**, e59203.

Lindsley, D. L. and Zimm, G. G. (1992). *The Genome of Drosophila melanogaster*. Cambridge: Academic Press.

Lopes, C. S. and Casares, F. (2010). hth maintains the pool of eye progenitors and its downregulation by Dpp and Hh couples retinal fate acquisition with cell cycle exit. *Dev. Biol.* **339**, 78-88.

Lopes, C. S. and Casares, F. (2015). Eye selector logic for a coordinated cell cycle exit. *PLoS Genet.* **11**, e1004981.

Mardon, G., Solomon, N. M. and Rubin, G. M. (1994). dachshund encodes a nuclear protein required for normal eye and leg development in Drosophila. *Development* **120**, 3473-3486.

Morillo, S. A., Braid, L. R., Verheyen, E. M. and Rebay, I. (2012). Nemo phosphorylates Eyes absent and enhances output from the Eya-Sine oculis transcriptional complex during Drosophila retinal determination. *Dev. Biol.* **365**, 267-276.

Mutsuddi, M., Chaffee, B., Cassidy, J., Silver, S. J., Tootle, T. L. and Rebay, I. (2005). Using Drosophila to decipher how mutations associated with human branchio-oto-renal syndrome and optical defects compromise the protein tyrosine phosphatase and transcriptional functions of eyes absent. *Genetics* **170**, 687-695.

Niimi, T., Seimiya, M., Kloter, U., Flister, S. and Gehring, W. J. (1999). Direct regulatory interaction of the eyeless protein with an eye-specific enhancer in the sine oculis gene during eye induction in Drosophila. *Development* **126**, 2253-2260.

Ohto, H., Kamada, S., Tago, K., Tominaga, S.-I., Ozaki, H., Sato, S. and Kawakami, K. (1999). Cooperation of six and eya in activation of their target genes through nuclear translocation of Eya. *Mol. Cell. Biol.* **19**, 6815-6824.

O'Neill, E. M., Rebay, I., Tjian, R. and Rubin, G. M. (1994). The activities of two Ets-related transcription factors required for Drosophila eye development are modulated by the Ras/MAPK pathway. *Cell* **78**, 137-147.

Pappu, K. S. (2003). Mechanism of hedgehog signaling during Drosophila eye development. *Development* **130**, 3053-3062.

Pappu, K. S., Ostrin, E. J., Middlebrooks, B. W., Sili, B. T., Chen, R., Atkins, M. R., Gibbs, R. and Mardon, G. (2005). Dual regulation and redundant function of two eye-specific enhancers of the Drosophila retinal determination gene dachshund. *Development* **132**, 2895-2905.

Peng, H. W., Slattery, M. and Mann, R. S. (2009). Transcription factor choice in the Hippo signaling pathway: Homothorax and yorkie regulation of the microRNA bantam in the progenitor domain of the Drosophila eye imaginal disc. *Genes Dev.* **23**, 2307-2319.

Pignoni, F., Hu, B., Zavitz, K. H., Xiao, J., Garrity, P. A. and Zipursky, S. L. (1997). The eye-specification proteins So and Eya form a complex and regulate multiple steps in Drosophila eye development. *Cell* **91**, 881-891.

Ray, P., De, S., Mitra, A., Bezstarosti, K., Demmers, J. A. A., Pfeifer, K. and Kassis, J. A. (2016). Combgap contributes to recruitment of Polycomb group proteins in *Drosophila*. *Proc. Natl. Acad. Sci. USA* **113**, 3826-3831.

Ready, D. F., Hanson, T. E. and Benzer, S. (1976). Development of the Drosophila retina, a neurocrystalline lattice. *Dev. Biol.* **53**, 217-240.

Ruggiero, R., Kale, A., Thomas, B. and Baker, N. E. (2012). Mitosis in neurons: roughex and APC/C maintain cell cycle exit to prevent cytokinetic and axonal defects in drosophila photoreceptor neurons. *PLoS Genet.* **8**, e1003049.

Salzer, C. L. and Kumar, J. P. (2009). Position dependent responses to discontinuities in the retinal determination network. *Dev. Biol.* **326**, 121-130.

Silver, S. J., Davies, E. L., Doyon, L. and Rebay, I. (2003). Functional dissection of eyes absent reveals new modes of regulation within the retinal determination gene network. *Mol. Cell. Biol.* **23**, 5989-5999.

Song, Y., Chung, S. and Kunes, S. (2000). Combgap relays wingless signal reception to the determination of cortical cell fate in the Drosophila visual system. *Mol. Cell* **6**, 1143-1154.

Staehling-Hampton, K., Clark, M. J., Hoffmann, F. M., Jackson, P. D. and Brand, H. (1994). Specificity of bone morphogenetic factors: cell fate and gene expression changes in drosophila embryos induced by decapentaplegic but not 60A. *Cell Growth Differ.* **5**, 585-593.

Stowers, R. S. and Schwarz, T. L. (1999). A genetic method for generating Drosophila eyes composed exclusively of mitotic clones of a single genotype. *Genetics* **152**, 1631-1639.

Sukhanova, M. J. and Du, W. (2008). Control of cell cycle entry and exiting from the second mitotic wave in the Drosophila developing eye. *BMC Dev. Biol.* **10**, 1-10.

Svendsen, P. C., Marshall, S. D., Kyba, M. and Brook, W. J. (2000). The combgap locus encodes a zinc-finger protein that regulates cubitus interruptus during limb development in Drosophila melanogaster. *Development* **127**, 4083-4093.

Szklarczyk, D., Franceschini, A., Wyder, S., Forslund, K., Heller, D., Huerta-Cepas, J., Simonovic, M., Roth, A., Santos, A., Tsafou, K. P. et al. (2015). STRING v10: protein–protein interaction networks, integrated over the tree of life. *Nucleic Acids Res.* **43**, D447-D452.

Thorvaldsdóttir, H., Robinson, J. T. and Mesirov, J .P. (2013). Integrative Genomics Viewer (IGV): High-performance genomics data visualization and exploration. *Brief. Bioinform.* **14**, 178-192.

Vrailas, A. D. and Moses, K. (2006). Smoothened, thickveins and the genetic control of cell cycle and cell fate in the developing Drosophila eye. *Mech. Dev.* **123**, 151-165.

Weasner, B. M. and Kumar, J. P. (2013). Competition among gene regulatory networks imposes order within the eye-antennal disc of Drosophila. *Development* **140**, 205-215.

Webber, J. L., Zhang, J., Mitchell-Dick, A. and Rebay, I. (2013). 3D chromatin interactions organize Yan chromatin occupancy and repression at the even-skipped locus. *Genes Dev.* **27**, 2293-2298.

Wolff, T. and Ready, D. F. (1991). The beginning of pattern formation in the Drosophila compound eye: the morphogenetic furrow and the second mitotic wave. *Development* **850**, 841-850.

Development (2017) 144, 2640-2651 doi:10.1242/dev.147231

Xin, S., Weng, L., Xu, J. and Du, W. (2002). The role of RBF in developmentally regulated cell proliferation in the eye disc and in Cyclin D/Cdk4 induced cellular growth. *Development* **129**, 1345-1356.

Xu, P.-X., Cheng, J., Epstein, J. A. and Maas, R. L. (1997). Mouse Eya genes are expressed during limb tendon development and encode a transcriptional activation function. *Proc. Natl. Acad. Sci. USA* **94**, 11974-11979.

Yan, H., Canon, J. and Banerjee, U. (2003). A transcriptional chain linking eye specification to terminal determination of cone cells in the Drosophila eye. *Dev. Biol.* **263**, 323-329.

Yang, L. and Baker, N. E. (2003). Cell cycle withdrawal, progression, and cell survival regulation by EGFR and its effectors in the differentiating Drosophila eye. *Dev. Cell* **4**, 359-369.

Yang, L. and Baker, N. E. (2006). Notch activity opposes ras-induced differentiation during the second mitotic wave of the developing Drosophila eye. *BMC Cell Biol.* **6**, 8.

Zhang, T., Ranade, S., Cai, C. Q., Clouser, C. and Pignoni, F. (2006). Direct control of neurogenesis by selector factors in the fly eye: regulation of atonal by Ey and So. *Development* **133**, 4881-4889.

Zhou, Q., Zhang, T., Jemc, J. C., Chen, Y., Chen, R., Rebay, I. and Pignoni, F. (2014). Onset of atonal expression in Drosophila retinal progenitors involves redundant and synergistic contributions of Ey/Pax6 and So binding sites within two distant enhancers. *Dev. Biol.* **386**, 152-164.

Zhu, L. and Skoultchi, A. I. (2001). Coordinating cell proliferation and differentiation. *Curr. Opin. Genet. Dev.* **11**, 91-97.

Supplementary Materials & Methods

Drosophila strains & genetics

UAS-cg flies were made by amplifying the coding region from BDGP DGC cDNA clone LD05357 with oligos 5'- CATGGTACCTGTGCCGCCCAGAATCCGCC-3' and 5'-CACTCTAGACTAGCATACCTGTTGCTGCGATATGGCTG-3', subcloning into pUASt-FLAG-attB and integrating into the ϕC31 86FB landing site (Bischof et al., 2007).

The *RNAi* transgenes targeting *cg* are predicted to degrade hundreds of off-target transcripts and produced phenotypes we never observed in *cg* mutants (data not shown), while the perdurance of maternally deposited Cg protein (Ray et al., 2016) masked the null phenotype in all but the earliest-generated mitotic clones. We bypassed these problems by hand-picking first instar homozygous *cg* mutant larvae. These animals normally die at early larval stages when faced with competition from their heterozygous siblings, but when isolated and cultured independently, a small fraction survive to the late third instar, enabling analysis of their eye-antennal discs.

To determine the roles of *eya* and *so* and to assess their interactions with other genes in the SMW, we crossed *GMR-GAL4^{Zipursky}/CyO,act-GFP* or *GMR-GAL4^{Zipursky},UAS-eya^{RNAi}/CyO,dfd-YFP* to *w^{1118}*, *UAS-so^{RNAi}*, *UAS-stg^{RNAi}*, *pnt$^{\Delta 88}$/TM3,Ser,twi-GAL4,UAS-GFP*, *ttk^{1e11}/TM6B,Hu,Tb*, *FRT42D,cg^{A22}/CyO,dfd-YFP*, or *UAS-cg*. Genetic interactions between *eya* and *cg* were assessed by crossing *ey-GAL4*, *ey-GAL4,UAS-eya^{RNAi}*, *GMR-GAL4^{Zipursky}/CyO,act-GFP*, or *GMR-GAL4^{Zipursky},UAS-eya^{RNAi}/CyO,dfd-YFP* to *w^{1118}*, *FRT42D,cg^{A22}/CyO,dfd-YFP*, or *Df(2R)BSC401/CyO*. For ectopic Dac induction experiments, we crossed *dpp^{40C6}-GAL4/TM6B,Hu,Tb*, *dpp^{40C6}-GAL4,UAS-eya^{IIIa}/TM6B,Hu,Tb*, *dpp^{57A1}-GAL4/CyO,dfd-YFP*, or *dpp^{57A1}-GAL4,UAS-eya^{1}/CyO,dfd-YFP* to *w^{1118}*, *FRT42D,cg^{A22}/CyO,dfd-YFP*, or *UAS-cg*. To determine the role of *cg* in the eye-antennal imaginal disc, including the SMW, and to assess its genetic interaction with *eya* and *so*, we crossed *FRT42D,cg^{A22}/CyO,dfd-YFP* to *eya^{Clift},FRT42D,cg^{A22}/CyO,dfd-YFP* or *FRT42D,so^{3},cg^{A22}/CyO,dfd-YFP* and compared with *w^{1118}*. Mitotic or whole-eye clones were made by crossing *ey-FLP;FRT42D,ubi-GFP/CyO* or

y^1,w^*;FRT42D,y^+,GMR-hid,l(2)CL-R^1/Cyo;ey-GAL4,UAS-FLP to *FRT42D*, *FRT42D,cg^{A22}/CyO,dfd-YFP*, *eya^{Clift},FRT42D,cg^{A22}/CyO,dfd-YFP*, or *eya^{A188},FRT42D,cg^{A22}/CyO,dfd-YFP*. Flies were reared on standard cornmeal-molasses-agar medium and all crosses were at 25°C.

Immunohistochemistry & Microscopy

Primary antibodies: rabbit α-PH3 (1:2000, Upstate, 06-570), rat α-ELAV (1:50, Developmental Studies Hybridoma Bank [DSHB], 7E8A10) (O'Neill et al., 1994), guinea pig α-Eya (1:1000) (Silver et al., 2003), mouse α-Dac (1:10, DSHB, mAbdac2-3) (Mardon et al., 1994), rabbit α-FLAG (1:500, Sigma, F1804), mouse α-Delta (1:1000, DSHB, C594.9B) (Fehon et al., 1990), mouse α-Cut (1:100, DSHB, 2B10) (Blochlinger et al., 1990), rabbit α-cleaved caspase 3 (1:1000, Cell Signaling), and mouse α-Pros (1:100, DSHB, MR1A) (Campbell et al., 1994). Secondary antibodies were from Jackson ImmunoResearch: donkey α-rabbit-Cy3 (1:2000), donkey α-rabbit-488 (1:2000), donkey α-rat-Cy3 (1:2000), donkey α-rat-488 (1:2000), donkey α-mouse-Cy3 (1:2000), or donkey α-guinea pig-488 (1:2000). Oregon Green 488 Phalloidin (1:2000, Thermo Fisher Scientific) and DAPI (1:2000, Invitrogen) were used to detect actin and DNA, respectively. The Click-iT EdU Alexa Fluor 594 Imaging Kit (Molecular Probes, C10339) was used to label DNA synthesis.

For antibody staining, third instar eye-antennal imaginal discs were dissected in S2 cell medium, fixed for 10 min in 4% paraformaldehyde with 0.1% Triton X-100, washed 3X in PBT (1X PBS, 0.1% Triton), blocked in PNT (1X PBS, 0.1% Triton, 1% normal goat serum), stained with primary antibodies in PNT overnight at 4° C, washed 3X in PBT, and stained with secondary antibodies in PNT for 2 h at room temperature or overnight at 4° C. Pupal and adult tissues were treated in the same manner, except that halved heads were fixed for 20 min prior to dissecting the retinas, and then post-fixed for 10 min.

For S-phase detection, dissected discs were incubated in 10 μM EdU in PBS for 60 min at room temperature, rinsed 5 min in PBS, fixed for 15 min in 4% paraformaldehyde in PBS, washed 3X 5 min in PBS with 0.3% Triton X-100 (PBT3), washed 20 min in PBS

with 0.6% Triton X-100 (PBT6), washed 2X 5 min in PBT3 with 3% BSA (PBT3B), incubated in the Click-iT reaction mixture 30 min in the dark, washed 5 min in PBT3B; washed 2X 5 min in PBT and mounted.

All primary antibodies used in this study are standard reagents in the fly eye field and have been subject to extensive prior validation. Additional validation of antibody specificity from our study included comparison of expression pattern, levels and subcellular localization in wild type versus mutant or overexpressed imaginal tissues and in transiently transfected S2 cells, as well as recapitulation of previously described and published expression patterns.

In vitro *pulldown assays*

GST-fusion proteins were expressed in BL21 *E. coli* cells, bound by Protino Glutathione Agarose 4B (Machery-Nagel), washed, and cleaved by TEV protease as necessary. Pulldown assays were performed by mixing equimolar amounts of the desired proteins in binding buffer (20 mM Tris, 100 mM NaCl, 0.1 mM EDTA, 2.5 mM $MgCl_2$, 0.1% NP-40, 10% glycerol, 100 ug/mL BSA). Binding reactions were incubated at 4° C for 2 h in the presence of glutathione sepharose resin, washed 3X in binding buffer with either 100 mM, 500 mM, or 1 M NaCl, boiled, resolved by SDS-PAGE, immunoblotted and imaged on a Li-COR Odyssey.

Transcription Assays in cultured S2 cells

2.25 x 10^6 of *Drosophila* S2 cells plated in 12-well plates in 1.5 mL of Schneider's medium (Sigma) with 10% insect medium supplement (Sigma), penicillin (Invitrogen), and streptomycin (Invitrogen) were transfected in duplicate with a mixture of dimethyl-dioctadecyl-ammonium bromide (DDAB) (Sigma) containing 750 ng of total plasmid DNA. After 48 h, cells were lysed in 100 mM KH_2PO_4, 0.5% NP-40, and 1 mM DTT at pH 7.8, incubated 1 h on ice, spun, and loaded into a tube luminometer in triplicate 50 µL aliquots (EG&G Berthold Autolumat LB953). Firefly and Renilla luciferases were activated by exposure of lysates to 100 µL of 0.01 M Magnesium acetate, 0.1 M Tris acetate, 1 mM EDTA, 76.9 µM luciferin (BD Pharmingen), and 4.62 mM ATP (Fisher) at pH 7.8 or 25 mM Sodium pyrophosphate, 10 mM Sodium acetate, 15 mM EDTA, 0.5 M

Na_2SO_4, 0.5 M NaCl, and 4 μM coelenterazine (Promega) at pH 5.0, respectively. Empty vector was used to standardize the amount of DNA transfected across conditions, and all measurements were normalized to the activity of Renilla luciferase expressed under the control of an *actin* promoter.

To generate the 2X-LMEE reporter, we inserted a SalI restriction site into the multiple cloning site of pBS-TATA-luciferase (Silver et al. 2003) and ligated in two copies of the *LMEE* sequence amplified with 5'-CAGCTCGAGAGCGCACATTCTTGCCACATCCTTG-3' and 5'-GCGGTCGACCATTAACAAAATAAAAAAGGGGAACGACTCGTGCG-3'. The Gateway system (Invitrogen) was used to insert the full-length *cg* cDNA, amplified with 5'-CGCGGATCCGGCTGTGCCGCCCAGAATCCG-3' and 5'-TGGCTCGAGAGTCTAGCATACCTGTTGCTGCGA-3' and subcloned into pENTR-3C, into the actin5C S2 cell expression vector pAFW.

S2 cells were replaced from frozen stocks every six months and were not authenticated or tested for contamination within that interval.

Supplementary Figures

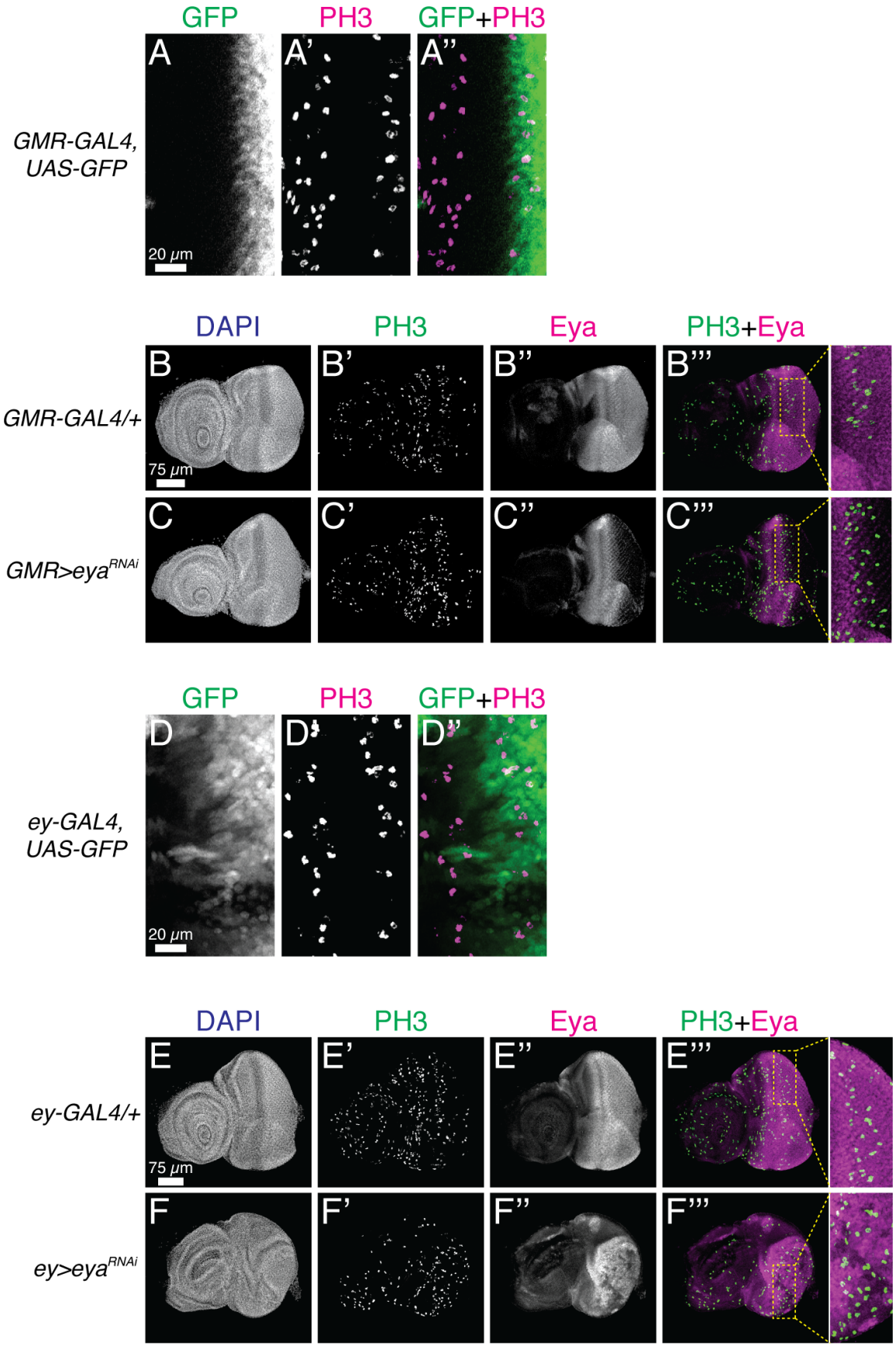

Fig. S1. Knockdown under *GMR-GAL4* depletes protein levels by the SMW. All images are maximum projections through representative third instar eye-antennal imaginal discs. Anterior is to the left and dorsal is up. PH3 was used to mark the SMW (A) *GMR-GAL4* drives GFP expressio in a domain overlapping the SMW. Panels are zoomed views centered on the MF. (B-C) *eya* knockdown under *GMR-GAL4* strongly reduces Eya protein levels at the SMW. (D) *ey-GAL4* drives GFP expression at and before the SMW. (E) *eya* knockdown under *ey-GAL4* lowers Eya protein levels before and in the SMW and increases SMW proliferation posterior to the MF.

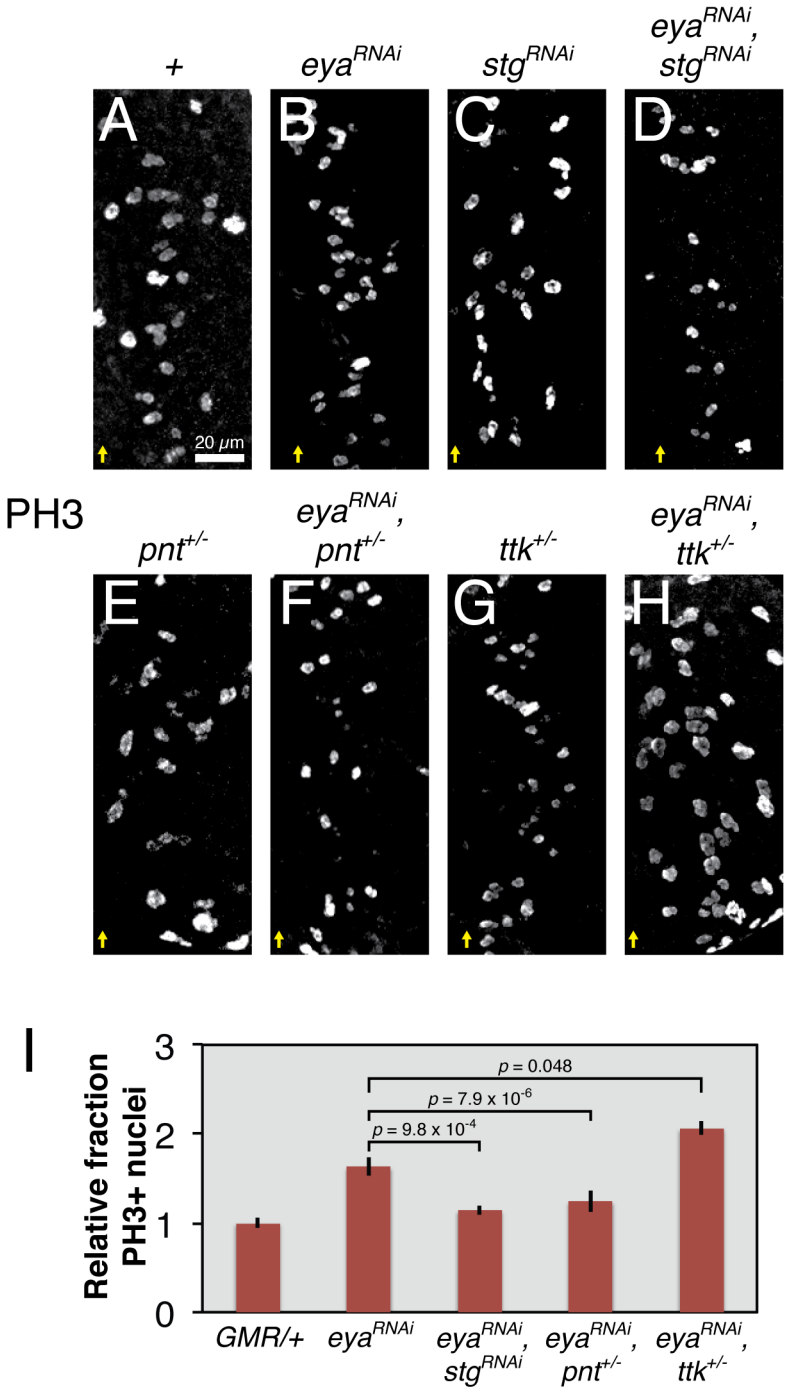

Fig. S2. Genetic interactions between *eya* and M phase regulators at the SMW. All images show representative late third instar eye-antennal imaginal discs. Yellow arrows mark the ventral edge of the MF. *UAS* transgenes were expressed with *GMR-GAL4*. (A-D) Dominant suppression of the increased SMW mitotic rate in *eya* knockdown discs by weak *string* knockdown that on its own does not impair the SMW. (T-W) Dominant suppression and enhancement of the *eya*

knockdown SMW phenotype by reducing the dose of *pnt* or *ttk*, respectively. (X) Quantification of mitotic rates for genotypes in P-W ($n \geq 7$), calculated as in G. Actual PH3 counts for C-F and P-W in Supplementary Table 1.

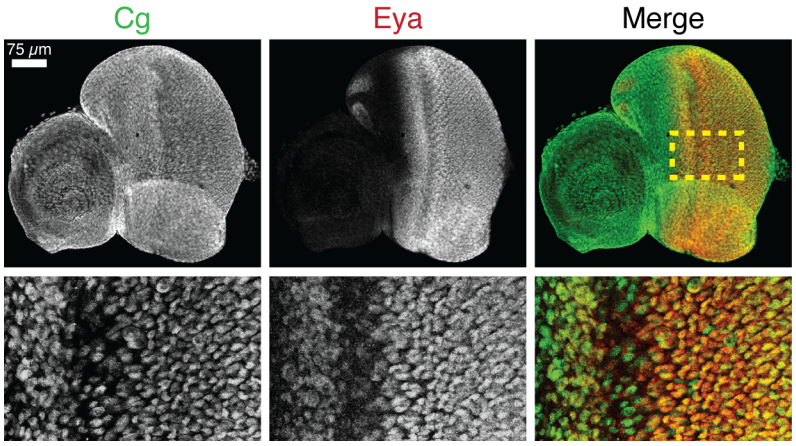

Fig. S3. Cg and Eya are co-expressed in the eye imaginal disc. A homozygous *cg-GFP* disc was stained with rabbit anti-GFP and guinea pig anti-Eya. The top row shows maximum confocal projections, while the zoomed views in the bottom row are partial projections focused on the photoreceptors. The yellow box shows the position of the zoomed panels in the disc.

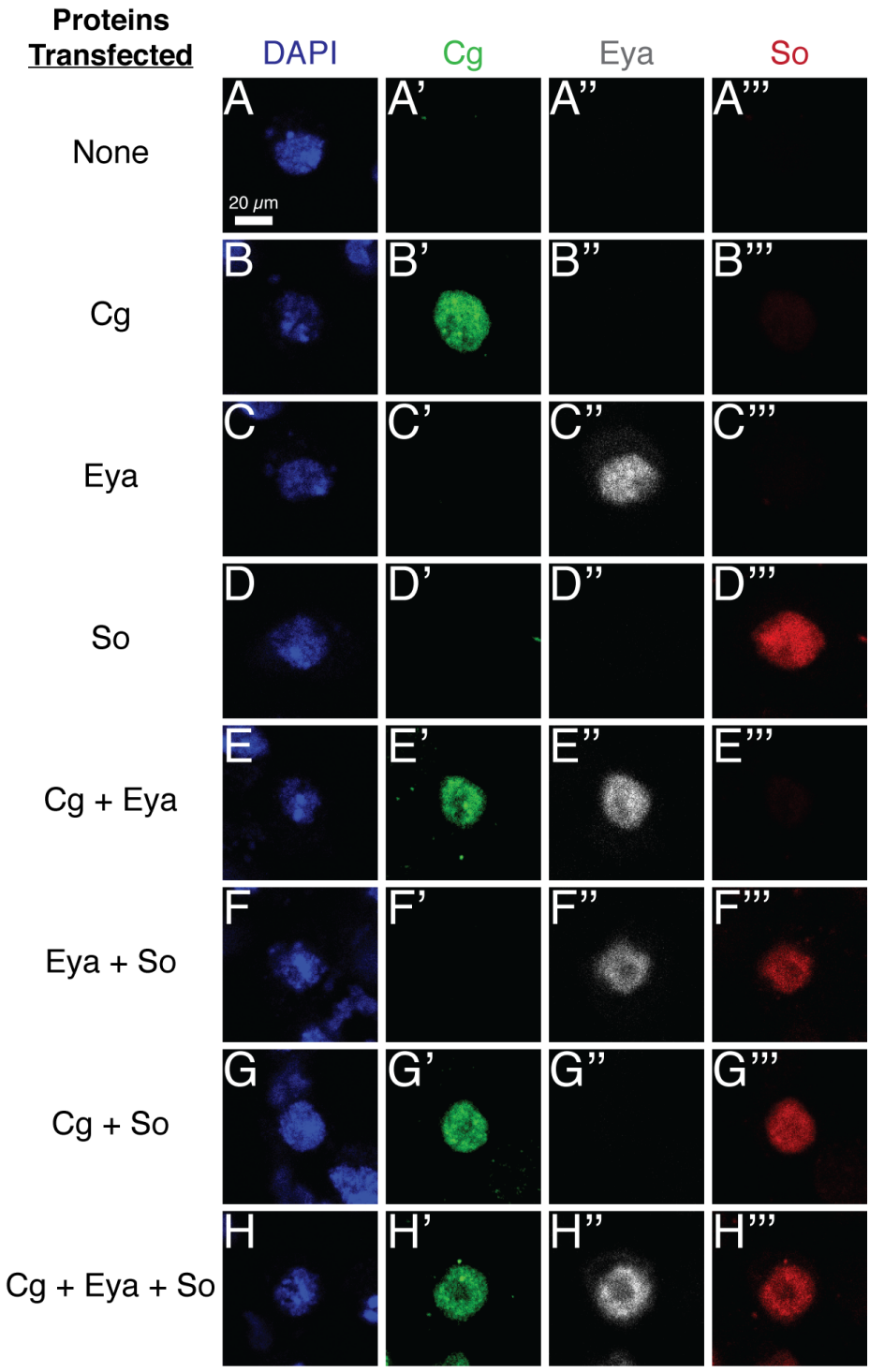

Fig. S4. Eya, So, and Cg co-localize in the nuclei of cultured S2 cells. All images are single confocal slices through the nuclei of representative S2 cells. Cells were transiently transfected with plasmids encoding the proteins indicated to the left of each row, fixed, and stained for the proteins indicated above each column.

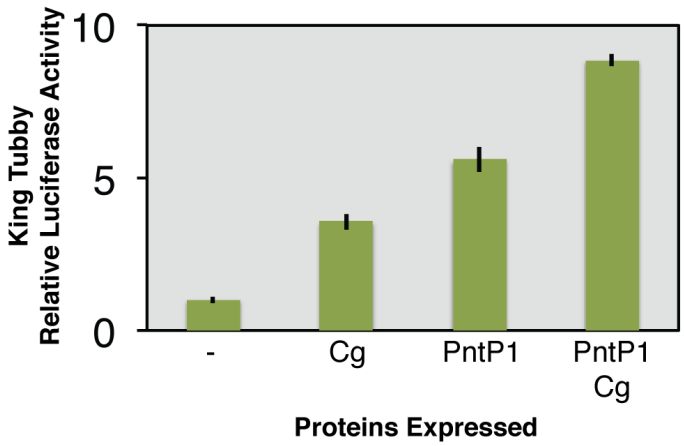

Fig. S5. Cg does not limit the ability of PntP1 to activate transcription. Experimental conditions are identical to Fig. 3A, except for expression of PntP1 and use of a Pnt-responsive *King Tubby* reporter (Webber et al., 2013). This experiment was replicated independently twice. Note that Cg alone activates expression of this reporter and additively increases output relative to PntP1 alone.

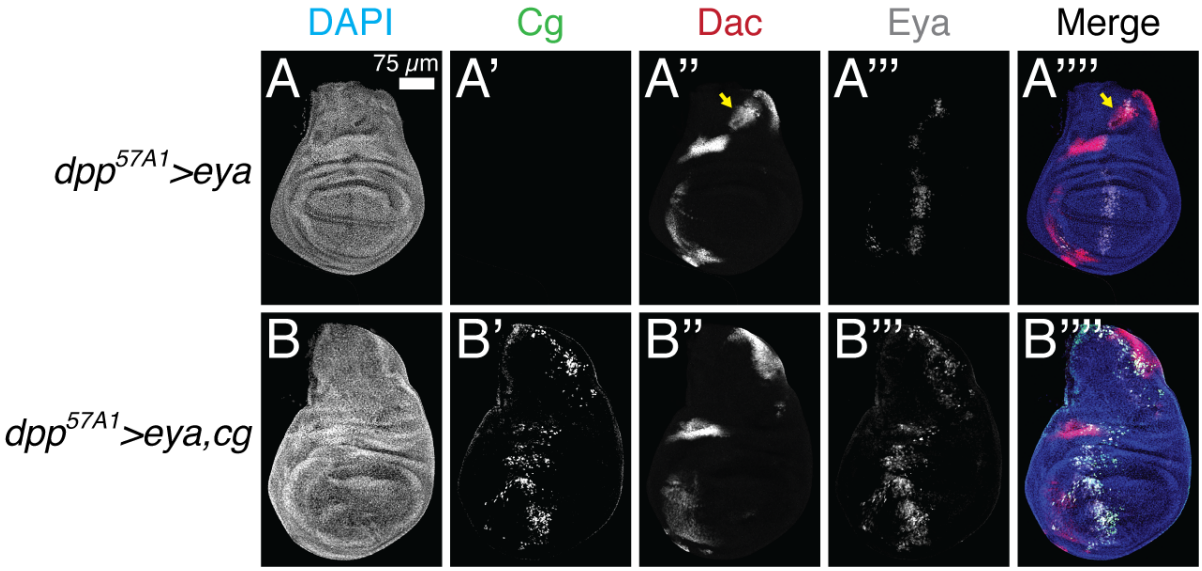

Fig. S6. Co-overexpressing *cg* does not reduce Eya levels in wing imaginal discs. Experimental and imaging conditions are identical to Fig. 3F and H, except that the tissue was also stained with guinea pig anti-Eya. The aberrant folding in discs co-overexpressing *eya* and *cg* expanded the Eya expression stripe, making the reduced induction of ectopic Dac even more striking.

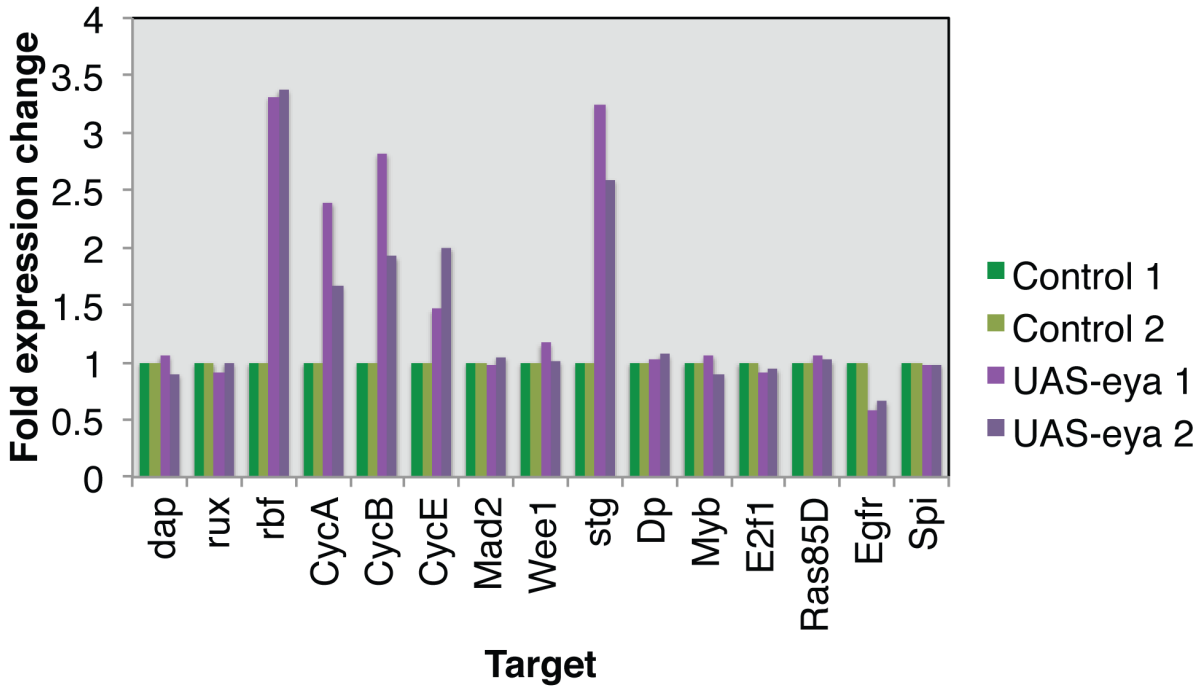

Fig. S7. The effect of *eya* overexpression on the transcription of cell cycle regulators in the eye-antennal imaginal disc. Raw data were obtained from Jemc et al., 2007. Two experimental replicates are shown. All bars are normalized to the control conducted with that replicate.

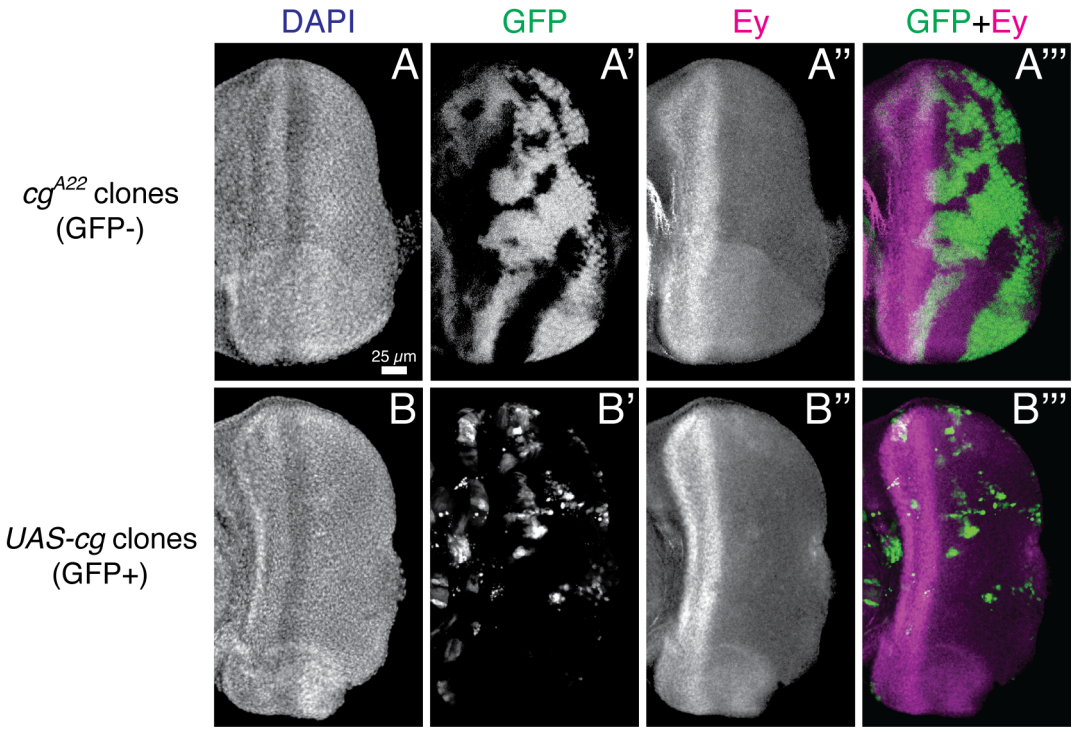

Fig. S8. *cg* does not control Ey expression in the eye imaginal disc. All images are maximum confocal projections of late third instar eye-antennal imaginal discs. Anterior is to the left and dorsal is up. (A) Mitotic *cg* clones do not affect Ey levels anterior to the MF or de-repress Ey posterior to the MF. (B) *FLP-out* clones overexpressing *cg* do not lower Ey levels in the preproneural domain or affect expression posterior to the MF.

Figure	Genotype	PH3+ Nuclei	MF length (μm)	PH3+ nuclei/μm MF	Normalization factor	Normalized
1G	*GMR-GAL4/+*	84	553.657	0.151718483	0.130309313	1.164295006
1G	*GMR-GAL4/+*	71	546.557	0.129904109	0.130309313	0.996890441
1G	*GMR-GAL4/+*	86	577.453	0.14892987	0.130309313	1.142895054
1G	*GMR-GAL4/+*	72	560.545	0.128446423	0.130309313	0.985704087
1G	*GMR-GAL4/+*	69	593.247	0.116309058	0.130309313	0.892561364
1G	*GMR-GAL4/+*	86	623.529	0.137924619	0.130309313	1.058440229
1G	*GMR-GAL4/+*	80	592.12	0.135107748	0.130309313	1.036823424
1G	*GMR-GAL4/+*	53	563.026	0.094134196	0.130309313	0.722390395
1G	*GMR-GAL4,UAS-eyaRNAi/+*	81	469.539	0.172509632	0.130309313	1.323847294
1G	*GMR-GAL4,UAS-eyaRNAi/+*	71	453.067	0.156709714	0.130309313	1.202597957
1G	*GMR-GAL4,UAS-eyaRNAi/+*	90	481.892	0.186763839	0.130309313	1.433234774
1G	*GMR-GAL4,UAS-eyaRNAi/+*	58	287.487	0.201748253	0.130309313	1.548225893
1G	*GMR-GAL4,UAS-eyaRNAi/+*	104	456.654	0.227743543	0.130309313	1.747715013
1G	*GMR-GAL4,UAS-eyaRNAi/+*	77	432.304	0.1781154	0.130309313	1.366866234
1G	*GMR-GAL4,UAS-eyaRNAi/+*	75	498.05	0.15058729	0.130309313	1.155614182
1G	*GMR-GAL4,UAS-eyaRNAi/+*	88	495.807	0.177488418	0.130309313	1.36205474
1G	*GMR-GAL4,UAS-eyaRNAi/+*	95	506.719	0.187480635	0.130309313	1.438735502
1G	*GMR-GAL4,UAS-eyaRNAi/+*	74	447.314	0.165431889	0.130309313	1.269532352
1G	*GMR-GAL4/UAS-soRNAi*	104	582.543	0.178527594	0.130309313	1.370029426
1G	*GMR-GAL4/UAS-soRNAi*	109	578.237	0.188504022	0.130309313	1.446589019
1G	*GMR-GAL4/UAS-soRNAi*	79	443.23	0.178237033	0.130309313	1.367799647
1G	*GMR-GAL4/UAS-soRNAi*	92	546.714	0.168278113	0.130309313	1.291374409
1G	*GMR-GAL4/UAS-soRNAi*	68	410.579	0.165619771	0.130309313	1.270974168
1G	*GMR-GAL4,UAS-eyaRNAi/UAS-soRNAi*	97	508.816	0.190638659	0.130309313	1.462970331
1G	*GMR-GAL4,UAS-eyaRNAi/UAS-soRNAi*	76	491.94	0.154490385	0.130309313	1.185566719
1G	*GMR-GAL4,UAS-eyaRNAi/UAS-soRNAi*	102	488.77	0.208687113	0.130309313	1.601475039
1G	*GMR-GAL4,UAS-eyaRNAi/UAS-soRNAi*	96	475.836	0.201750183	0.130309313	1.548240703
1G	*GMR-GAL4,UAS-eyaRNAi/UAS-soRNAi*	87	506.787	0.171669755	0.130309313	1.317402037
1G	*GMR-GAL4,UAS-eyaRNAi/UAS-soRNAi*	93	572.223	0.162524051	0.130309313	1.247217461
1G	*GMR-GAL4,UAS-eyaRNAi/UAS-soRNAi*	100	530.329	0.188562194	0.130309313	1.447035439
1G	*GMR-GAL4,UAS-eyaRNAi/UAS-soRNAi*	58	364.011	0.159335844	0.130309313	1.222751008
1G	*GMR-GAL4,UAS-eyaRNAi/UAS-soRNAi*	106	578.081	0.183365307	0.130309313	1.407154272
1G	*GMR-GAL4,UAS-eyaRNAi/UAS-soRNAi*	85	565.587	0.15028634	0.130309313	1.153304671
S2I	*GMR-GAL4/+*	56	546.87	0.102400936	0.102578397	0.99827
S2I	*GMR-GAL4/+*	56	507.89	0.110260096	0.102578397	1.074886127
S2I	*GMR-GAL4/+*	54	415.436	0.129983921	0.102578397	1.267166621
S2I	*GMR-GAL4/+*	50	473.211	0.105661111	0.102578397	1.030052274
S2I	*GMR-GAL4/+*	54	651.113	0.082934913	0.102578397	0.808502721
S2I	*GMR-GAL4/+*	58	576.345	0.100634169	0.102578397	0.981046418
S2I	*GMR-GAL4/+*	43	522.491	0.082298068	0.102578397	0.80229435
S2I	*GMR-GAL4/+*	56	526.049	0.106453962	0.102578397	1.03778149
S2I	*GMR-GAL4,UAS-eyaRNAi/+*	50	542.78	0.092118354	0.102578397	0.89802879
S2I	*GMR-GAL4,UAS-eyaRNAi/+*	57	305.253	0.186730352	0.102578397	1.820367224
S2I	*GMR-GAL4,UAS-eyaRNAi/+*	89	545.114	0.163268601	0.102578397	1.59164703
S2I	*GMR-GAL4,UAS-eyaRNAi/+*	81	502.32	0.161251792	0.102578397	1.571985882
S2I	*GMR-GAL4,UAS-eyaRNAi/+*	69	528.263	0.130616757	0.102578397	1.273335918
S2I	*GMR-GAL4,UAS-eyaRNAi/+*	100	504.654	0.198155568	0.102578397	1.931747561
S2I	*GMR-GAL4,UAS-eyaRNAi/+*	57	303.503	0.18780704	0.102578397	1.830863471
S2I	*GMR-GAL4,UAS-eyaRNAi/+*	87	435.5	0.199770379	0.102578397	1.947489773
S2I	*GMR-GAL4,UAS-eyaRNAi/+*	71	426.822	0.16634569	0.102578397	1.621644467
S2I	*GMR-GAL4,UAS-eyaRNAi/+*	87	466.761	0.186390894	0.102578397	1.817057972
S2I	*GMR-GAL4,UAS-eyaRNAi/UAS-stgRNAi*	62	535.699	0.115736636	0.102578397	1.128274951
S2I	*GMR-GAL4,UAS-eyaRNAi/UAS-stgRNAi*	60	470.661	0.127480288	0.102578397	1.242759609
S2I	*GMR-GAL4,UAS-eyaRNAi/UAS-stgRNAi*	50	436.585	0.114525236	0.102578397	1.116465446
S2I	*GMR-GAL4,UAS-eyaRNAi/UAS-stgRNAi*	64	461.825	0.138580631	0.102578397	1.35097287
S2I	*GMR-GAL4,UAS-eyaRNAi/UAS-stgRNAi*	50	496.471	0.100710817	0.102578397	0.981793633
S2I	*GMR-GAL4,UAS-eyaRNAi/UAS-stgRNAi*	57	580.011	0.098273998	0.102578397	0.958037962
S2I	*GMR-GAL4,UAS-eyaRNAi/UAS-stgRNAi*	44	408.776	0.107638413	0.102578397	1.049328284
S2I	*GMR-GAL4,UAS-eyaRNAi/UAS-stgRNAi*	82	611.203	0.134161645	0.102578397	1.30789376
S2I	*GMR-GAL4,UAS-eyaRNAi/pnt*	22	172.467	0.127560635	0.102578397	1.243542877
S2I	*GMR-GAL4,UAS-eyaRNAi/pnt*	63	445.858	0.141300593	0.102578397	1.377488806
S2I	*GMR-GAL4,UAS-eyaRNAi/pnt*	50	433.299	0.115393758	0.102578397	1.12493236
S2I	*GMR-GAL4,UAS-eyaRNAi/pnt*	42	350.635	0.11978268	0.102578397	1.167718386
S2I	*GMR-GAL4,UAS-eyaRNAi/pnt*	48	323.991	0.148152263	0.102578397	1.44428328
S2I	*GMR-GAL4,UAS-eyaRNAi/pnt*	49	376.237	0.130237058	0.102578397	1.269634367
S2I	*GMR-GAL4,UAS-eyaRNAi/pnt*	28	186.737	0.149943503	0.102578397	1.461745436
S2I	*GMR-GAL4,UAS-eyaRNAi/pnt*	46	417.809	0.110098155	0.102578397	1.073307424
S2I	*GMR-GAL4,UAS-eyaRNAi/pnt*	62	490.58	0.126381018	0.102578397	1.23204322
S2I	*GMR-GAL4,UAS-eyaRNAi/pnt*	39	366.191	0.106501798	0.102578397	1.038247833
S2I	*GMR-GAL4,UAS-eyaRNAi/ttk*	115	574.588	0.200143407	0.102578397	1.951126291
S2I	*GMR-GAL4,UAS-eyaRNAi/ttk*	105	504.722	0.208035314	0.102578397	2.028061661
S2I	*GMR-GAL4,UAS-eyaRNAi/ttk*	129	530.986	0.242944258	0.102578397	2.368376436
S2I	*GMR-GAL4,UAS-eyaRNAi/ttk*	122	542.435	0.224911741	0.102578397	2.192583895
S2I	*GMR-GAL4,UAS-eyaRNAi/ttk*	125	606.749	0.206015997	0.102578397	2.008376064
S2I	*GMR-GAL4,UAS-eyaRNAi/ttk*	92	492.543	0.186785722	0.102578397	1.820907011
4G	*GMR-GAL4/+*	56	546.87	0.102400936	0.102578397	0.99827
4G	*GMR-GAL4/+*	56	507.89	0.110260096	0.102578397	1.074886127
4G	*GMR-GAL4/+*	54	415.436	0.129983921	0.102578397	1.267166621
4G	*GMR-GAL4/+*	50	473.211	0.105661111	0.102578397	1.030052274
4G	*GMR-GAL4/+*	54	651.113	0.082934913	0.102578397	0.808502721
4G	*GMR-GAL4/+*	58	576.345	0.100634169	0.102578397	0.981046418
4G	*GMR-GAL4/+*	43	522.491	0.082298068	0.102578397	0.80229435
4G	*GMR-GAL4/+*	56	526.049	0.106453962	0.102578397	1.03778149
4G	*GMR-GAL4,UAS-eyaRNAi/+*	50	542.78	0.092118354	0.102578397	0.89802879
4G	*GMR-GAL4,UAS-eyaRNAi/+*	57	305.253	0.186730352	0.102578397	1.820367224
4G	*GMR-GAL4,UAS-eyaRNAi/+*	89	545.114	0.163268601	0.102578397	1.59164703
4G	*GMR-GAL4,UAS-eyaRNAi/+*	81	502.32	0.161251792	0.102578397	1.571985882
4G	*GMR-GAL4,UAS-eyaRNAi/+*	69	528.263	0.130616757	0.102578397	1.273335918
4G	*GMR-GAL4,UAS-eyaRNAi/+*	100	504.654	0.198155568	0.102578397	1.931747561
4G	*GMR-GAL4,UAS-eyaRNAi/+*	57	303.503	0.18780704	0.102578397	1.830863471
4G	*GMR-GAL4,UAS-eyaRNAi/+*	87	435.5	0.199770379	0.102578397	1.947489773
4G	*GMR-GAL4,UAS-eyaRNAi/+*	71	426.822	0.16634569	0.102578397	1.621644467
4G	*GMR-GAL4,UAS-eyaRNAi/+*	87	466.761	0.186390894	0.102578397	1.817057972
4G	*GMR-GAL4,UAS-eyaRNAi/cg*	56	495.476	0.113022629	0.102578397	1.101817071
4G	*GMR-GAL4,UAS-eyaRNAi/cg*	53	466.863	0.113523668	0.102578397	1.106701518
4G	*GMR-GAL4,UAS-eyaRNAi/cg*	64	460.657	0.138932004	0.102578397	1.354398274
4G	*GMR-GAL4,UAS-eyaRNAi/cg*	58	536.181	0.108172427	0.102578397	1.054534192
4G	*GMR-GAL4,UAS-eyaRNAi/cg*	63	611.002	0.103109319	0.102578397	1.005175767
4G	*GMR-GAL4/cg*	68	652.935	0.104145129	0.102578397	1.015273512
4G	*GMR-GAL4/cg*	57	554.549	0.102786228	0.102578397	1.002026072
4G	*GMR-GAL4/cg*	57	536.036	0.106336142	0.102578397	1.036632906
4G	*GMR-GAL4/cg*	49	520.675	0.094108609	0.102578397	0.917431076
4G	*GMR-GAL4/cg*	62	520.633	0.119085805	0.102578397	1.160924803
4G	*GMR-GAL4/cg*	55	403.476	0.136315419	0.102578397	1.328890129

Figure	Genotype	PH3+ Nuclei	MF length (μm)	PH3+ nuclei/μm MF	Normalization factor	Normalized
4K	*w1118*	30	474.36	0.063243107	0.073939409	0.855336925
4K	*w1118*	34	442.618	0.076815674	0.073939409	1.038900301
4K	*w1118*	37	517.855	0.071448572	0.073939409	0.966312454
4K	*w1118*	35	523.093	0.066909708	0.073939409	0.9049262
4K	*w1118*	46	503.944	0.091279983	0.073939409	1.23452412
4K	*cg*	29	488.364	0.059381936	0.073939409	0.803116192
4K	*cg*	35	523.413	0.066868802	0.073939409	0.904372954
4K	*cg*	29	524.637	0.055276315	0.073939409	0.747589355
4K	*cg*	50	420.637	0.118867337	0.073939409	1.607631694
4K	*cg*	37	433.189	0.085413065	0.073939409	1.155176461
4K	*w1118*	25	486.592	0.051377746	0.079716795	0.6445034
4K	*w1118*	41	425.862	0.096275319	0.079716795	1.207716879
4K	*w1118*	43	505.89	0.084998715	0.079716795	1.066258557
4K	*w1118*	38	556.629	0.068268092	0.079716795	0.8563828
4K	*w1118*	45	491.34	0.091586274	0.079716795	1.148895586
4K	*w1118*	25	286.856	0.087151742	0.079716795	1.093267
4K	*w1118*	21	348.586	0.060243383	0.079716795	0.755717575
4K	*w1118*	37	583.373	0.063424259	0.079716795	0.795619773
4K	*w1118*	45	497.627	0.090429177	0.079716795	1.134380484
4K	*w1118*	38	536.913	0.070774967	0.079716795	0.887830061
4K	*w1118*	48	559.981	0.085717194	0.079716795	1.075271448
4K	*w1118*	56	563.387	0.099398815	0.079716795	1.24689928
4K	*w1118*	55	577.684	0.095207761	0.079716795	1.194324988
4K	*w1118*	22	312.874	0.070315846	0.079716795	0.882070657
4K	*w1118*	29	359.879	0.08058264	0.079716795	1.010861512
4K	*cg*	7	318.452	0.021981335	0.079716795	0.27574283
4K	*cg*	4	305.762	0.01308207	0.079716795	0.164106827
4K	*cg*	19	341.995	0.055556368	0.079716795	0.696921741
4K	*cg*	19	323.141	0.058797862	0.079716795	0.73758437
4K	*cg*	24	345.843	0.069395651	0.079716795	0.870527351
4K	*cg*	6	497.179	0.012068088	0.079716795	0.151387021
4K	*cg*	14	295.148	0.04743383	0.079716795	0.595029311
4K	*cg*	9	447.52	0.020110833	0.079716795	0.252278494
4K	*cg*	19	454.301	0.041822492	0.079716795	0.524638402
4K	*cg*	16	389.32	0.041097298	0.079716795	0.515541269
4K	*cg*	14	327.433	0.042756839	0.079716795	0.536359228
4P	*w1118*	69	474.36	0.145459145	0.118448256	1.228039565
4P	*w1118*	68	442.618	0.153631348	0.118448256	1.297033431
4P	*w1118*	57	517.855	0.110069421	0.118448256	0.929261642
4P	*w1118*	61	523.093	0.116614063	0.118448256	0.984514814
4P	*w1118*	41	503.944	0.081358246	0.118448256	0.686867404
4P	*w1118*	54	407.467	0.13252607	0.118448256	1.118852011
4P	*w1118*	42	574.301	0.073132382	0.118448256	0.617420502
4P	*w1118*	69	511.887	0.134795375	0.118448256	1.138010631
4P	*cg*	20	515.697	0.038782463	0.118448256	0.32742114
4P	*cg*	18	488.364	0.036857754	0.118448256	0.311171774
4P	*cg*	40	523.413	0.076421487	0.118448256	0.645188789
4P	*cg*	39	524.637	0.074337113	0.118448256	0.627591451
4P	*cg*	22	420.637	0.052301628	0.118448256	0.441556758
4P	*cg*	26	460.123	0.05650663	0.118448256	0.477057509
4P	*cg*	26	433.189	0.060019991	0.118448256	0.506719077
4P	*cg*	31	454.528	0.068202619	0.118448256	0.575800955
4P	*cg*	16	514.268	0.031112183	0.118448256	0.262664762
4P	*cg,eya/cg*	16	182.531	0.087656343	0.079716795	1.099596929
4P	*cg,eya/cg*	16	207.106	0.077255125	0.079716795	0.969119808
4P	*cg,eya/cg*	24	293.887	0.081664041	0.079716795	1.024427043
4P	*cg,eya/cg*	31	371.614	0.083419893	0.079716795	1.046453164
4P	*cg,eya/cg*	19	346.394	0.054850835	0.079716795	0.688071245
4P	*cg,eya/cg*	22	264.687	0.08311704	0.079716795	1.042654058
4P	*cg,eya/cg*	19	268.543	0.07075217	0.079716795	0.887544083
4P	*cg,eya/cg*	32	322.333	0.099276214	0.079716795	1.245361331
4P	*cg,eya/cg*	35	372.252	0.094022329	0.079716795	1.17945445
4P	*cg,eya/cg*	30	295.35	0.101574403	0.079716795	1.27419075
4P	*cg,eya/cg*	34	340.11	0.099967658	0.079716795	1.254035077
4P	*cg,eya/cg*	34	360.751	0.094247833	0.079716795	1.182283264
4P	*cg,eya/cg*	41	495.548	0.082736687	0.079716795	1.037882759
4P	*cg,eya/cg*	31	414.68	0.074756439	0.079716795	0.937775263
4P	*cg,so/cg*	37	517.049	0.071559949	0.118448256	0.604145229
4P	*cg,so/cg*	34	423.706	0.08024432	0.118448256	0.677463079
4P	*cg,so/cg*	39	290.777	0.1341234	0.118448256	1.132337485
4P	*cg,so/cg*	36	391.558	0.091940402	0.118448256	0.776207309
4P	*cg,so/cg*	29	418.977	0.06921621	0.118448256	0.584358202
4P	*cg,so/cg*	35	433.791	0.080684016	0.118448256	0.681175212
4P	*cg,so/cg*	31	266.749	0.116214119	0.118448256	0.981138285
4P	*cg,so/cg*	42	386.117	0.108775319	0.118448256	0.918336183
4P	*cg,so/cg*	41	381.308	0.107524626	0.118448256	0.907777195

Table S1. Raw counts of PH3$^+$ nuclei, measurements of MF length, and normalizations used to quantify the fraction of mitotic cells at the SMW. All PH3$^+$ nuclei in the SMW were manually counted using the multi-point selection tool in FIJI and divided by the length of the MF, measured with the segmented line tool, to obtain the number of mitotic cells per micron of the MF. Counts and measurements were carried out in unaltered confocal images to retain the three-dimensional nature of the tissue, and measurements included the entire length of the SMW,

including in cases where parts of the tissue folded under the rest of the disc. In rare instances where $PH3^{+}$ nuclei could not be resolved unambiguously, that portion of the disc was not analyzed. Figs. 1X and 4G present data for *GMR/+* and eya^{RNAi} from the same experiment that was carried out in parallel. Fig. 1G has the same sample sizes, but represents data from a different experiment.